https://doi.org/10.5194/egusphere-2026-5045
Preprint. Discussion started: 15 September 2026

Direct human forcing for earth system and climate impact modelling under CMIP7 scenarios

Dominik Paprotny[1,2,3], Maksym Bondarenko[4], Evgeny Noi[4,5], Andrew J. Tatem[4], Katja Frieler[3,6], Inga Sauer[3], Samir KC[7], Rob Dellink[8], Jarmo S. Kikstra[7], Laurence Hawker[4,5]

[1] Baltic Climate Centre, University of Szczecin, Szczecin, Poland
[2] Institute of Marine and Environmental Sciences, University of Szczecin, Szczecin, Poland
[3] Research Department Transformation Pathways, Potsdam Institute for Climate Impact Research (PIK), Member of the Leibniz Association, Potsdam, Germany
[4] WorldPop, University of Southampton, Southampton, United Kingdom
[5] School of Geographical Sciences, University of Bristol, United Kingdom
[6] Institute for Geography and Environmental Sciences, University of Potsdam, Potsdam, Germany
[7] Energy, Climate and Environment Program, International Institute for Applied Systems Analysis (IIASA), Laxenburg, Austria
[8] Environment Directorate, Organisation for Economic Co-operation and Development (OECD), Paris, France

Correspondence to: Dominik Paprotny (dominik.paprotny@usz.edu.pl)

Abstract. Direct human forcings are important input variables for earth system and climate impact models, describing societal influence on changes to climate and related risks. Here, we present a new multisource dataset consistently describing the spatial and temporal dynamics of the two most important direct human forcings: population and economic production. The dataset was created by harmonizing multiple datasets to achieve smooth transition both the historical (1850-2025) and future (2026-2100) time periods, and to cover many resolutions down to 1 km. Projections were produced for the latest Shared Socioeconomic Pathways (v3.2, 2025), applicable to the seven scenarios designed for Coupled Model Intercomparison Project Phase 7 (CMIP7) earth system models, which require population density as one of the inputs. In a further stage of CMIP7, the dataset will be applied to modelling (societal) climate impacts, particularly in the Inter-Sectoral Impact Model Intercomparison Project 4 (ISIMIP4). This requires additional variables such as population split by degree of urbanization, gross domestic product and fixed asset value, and high resolutions of the data. We show that the new data vastly improves upon quality and availability of direct human forcings compared to previous CMIP phases. It enables, for instance, process-based impact simulations across sectors, impact attribution research, risk assessment and socio-hydrology.

1 Introduction

Modelling the consequences of climate change requires specific input datasets known as “forcings” (Durack et al., 2025a). They define the exogenous drivers relevant to the historical and future variability of climate and its impacts. Earth system models operated under World Climate Research Programme’s Coupled Model Intercomparison Project (CMIP) use a set of

https://doi.org/10.5194/egusphere-2026-5045
Preprint. Discussion started: 15 September 2026

standardized data on natural and human influences known as "climate forcings" (Naik et al., 2025). In the ongoing CMIP phase 7 (CMIP7), a total of 12 climate forcings were defined, including population density (Durack et al., 2025b, Durack and Nicholls, 2026), which is for instance used in fire modelling (Li et al., 2026). Further downstream of the modelling chain, climate impact models use multiple forcing datasets to estimate the hazard, exposure and vulnerability components of multiple climate-induced risks. The outputs of earth system models constitute "climate-related forcings" that describe the hazard, while "direct human forcings" will be extended to cover land use change, agricultural and water management and to quantify exposure and vulnerability in particular (Frieler et al., 2026).

With the increasing resolution, accuracy and availability of climate-related forcings, there is growing need for improving direct human forcings even further to provide better estimates of climate impacts (Frieler et al., 2024). Further, the introduction of new scenarios of possible future climate change trajectories in ScenarioMIP-CMIP7 (The Scenario Model Intercomparison Project for CMIP7; van Vuuren et al., 2026) also requires a new update of such forcing data. There is also a desire for greater timeliness of input data under accelerating global warming (Naik et al., 2025), which would necessitate transparent, reproducible and efficient means of delivering frequent updates. Global exposure data published under the scenarios of previous CMIP cycles (e.g. Jones and O'Neill, 2016, Murakami and Yamagata, 2019, Wang and Sun, 2022, Wang et al., 2022) in particular lacked harmonization with historical data and usually had limited reproducibility, and were in any case made obsolete by the start of CMIP7. In this study, we introduce a methodology of combining numerous data sources into a comprehensive and scalable dataset of essential direct human forcings: population and economic activity. The following principles had driven the design of this dataset:

- Consistency between population data used as climate forcing in earth system models and the data used in impact models as direct human forcing.
- Ability to generate consistent data across resolutions from very coarse (0.5º, or ~50 km) to very fine (30", or ~1 km) for different applications.
- Harmonization of historical data with future projections to avoid breaks in the timeseries, both for national aggregates and on the grid-cell level
- Homogenous treatment of demographic and economic data and consistency between the demographic data and labour data in the economic model to avoid spatial and temporal discontinuities.

The resulting work is the first to provide a high-resolution, gridded dataset of global population and economic activity under the historical and ScenarioMIP-CMIP7 scenarios, including updated population and economic estimates for the Shared Socioeconomic Pathways, or SSPs (IIASA, 2025). It covers the full time period of interest in CMIP7 (1850–2100), while additionally providing population projections up to year 2300 to support extended earth system model runs (van Vuuren et al., 2026). The dataset has already contributed to CMIP7 by providing population density as one of the climate forcings (Paprotny, 2026, Durack and Nicholls, 2026). It will find further applications in climate change studies, ranging from impact attribution and risk modeling, including the Inter-Sectoral Impact Model Intercomparison Project (ISIMIP, 2026a). In its fourth simulation

https://doi.org/10.5194/egusphere-2026-5045
Preprint. Discussion started: 15 September 2026

round (ISIMIP4) the impact models from different sectors will be forced by climate simulations and consistent direct human forcings from CMIP7-ScenarioMIP and particularly include the population and assets distribution described in this paper.

2 Methods

2.1 Framework of combining data

The global exposure dataset combines multiple input datasets to produce homogenized and gridded datasets (Fig. 1). The dataset is generated by an algorithm that combines three layers of input data:

(1) A database of national-level historical and projected timeseries of population, gross domestic product (GDP) and fixed asset value for all countries of the world for 1850–2100 (compiled in this study from multiple sources);

(2) A database of subnational-level historical GDP per capita for selected countries and available years during 1850–2023 (compiled in this study from multiple sources);

(3) External gridded datasets of population and built-up area combined and interpolated where necessary (Klein Goldewijk et al., 2017, Schiavina et al., 2023, Pesaresi et al., 2024, Bondarenko et al., 2025a, 2025b).

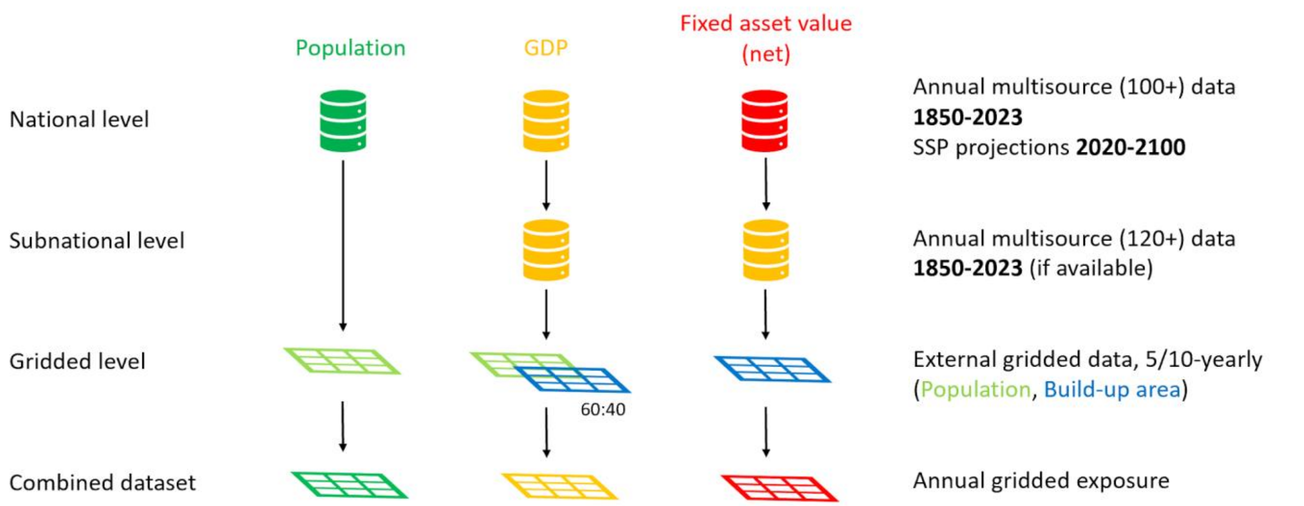

Figure 1. Framework of combining three layers of datasets into annual gridded exposure.

Historical data at national and subnational levels were compiled and harmonized from about 200 different sources for years 1850–2023 (sections 2.3.2–4). Through consistent application of national/subnational divisions (section 2.3.1), the data is downscalled to a 30” (~1 km) geographic grid using four external datasets (sections 2.3.2 and 2.3.5). SSP scenarios (section 2.2) provided further national-level data for future projections until 2100, with additional extension for population until 2300.

https://doi.org/10.5194/egusphere-2026-5045
Preprint. Discussion started: 15 September 2026

The population data is further disaggregated by degrees of urbanization, using a methodology developed by several statistical agencies (section 2.4). Finally, we compare the results with high-resolution population data from other sources to validate the approach (section 2.5).

2.2 2025 SSP scenarios

The scenario data used here are national scenario data following the Shared Socioeconomic Pathways (SSPs), which provide five internally consistent narratives of future societal development spanning divergent trajectories (O'Neill et al. 2017). For GDP, country-level projections are made for 196 countries (collectively representing more than 99% of global GDP), building on a range of country- and time-specific drivers, including investment; employment (as driven by demographic trends, labour participation rates and unemployment scenarios); human capital (as driven by education); energy rents and demand (as driven by energy efficiency and an assumption about future international oil prices); and total factor productivity (TFP), whereby each country gradually converges to its own frontier (Dellink et al., 2017). For the period 2010-2025, global net growth was roughly equally driven by capital and natural resources and by technology developments. The positive and negative effects of demographic developments more or less cancelled each other out. In high-income countries, some demographic trends, such as increased participation rates of older age groups and relatively low birth rates, implied that the positive effect on employment and human capital outweighed the negative effect on population as a driver of income growth. Capital accumulation as a driver of growth is especially strong in upper-middle income countries; these countries have the capacity to absorb additional capital and translate that into productive use. In low-income countries, the commodity slump in the middle of the last decade and other downward pressures on economic growth are reflected in the negative growth contribution of the "technology" group of drivers, which effectively includes all drivers that are not attributable elsewhere.

In the projections until the end of the century, SSP2 is the scenario that is closest to a "business-as-usual" baseline, although that should not be interpreted as a linear continuation of current trends; the global GDP per capita average annual growth rate is projected to slightly decline from 2.0% for 2010-2025 to 1.8% annually. SSP1 is the scenario with fast convergence and thus fast growth in low-income countries compared to higher income countries, leading to an average annual growth rate of GDP per capita of 2.0%. SSP3 is a low-growth scenario with almost no income growth in higher income countries but still some catch-up in low-income countries (global average annual growth rate 0.6%). SSP4 has fragmented growth: low-income countries follow a trajectory close to that of SSP3, while high-income countries are closer to an SSP2 or SSP1 trajectory (the global average annual growth rate, which is less meaningful in this scenario given the divergence, equals 1.3%). SSP5 has highest growth rates in all regions although as countries catch up relatively fast, and growth rates tend to stabilise; the global average annual growth rate peaks at around 3.4% in the 2030s and averages to 2.7% for the 2025-2100 period.

For population projections, the narrative elements of interest are fertility, mortality, migration, and educational attainment. The demographic human core of the SSPs, developed by KC and Lutz (2014) and updated in KC et al. (2024), projects population and human capital for 200 countries to 2100, disaggregated by age, sex, and six levels of educational attainment (KC, 2026a). SSP1 represents a world of rapid social progress, combining low fertility, low mortality, and fast educational

https://doi.org/10.5194/egusphere-2026-5045
Preprint. Discussion started: 15 September 2026

expansion. Under this pathway, the global population peaks below 9.3 billion around mid-century and declines to approximately 8.1 billion by 2100. The SSP5 pathway is almost identical to SSP1. SSP2 is the central continuation scenario, assuming medium fertility, mortality, and migration aligned with historical trends, and educational attainment. Global population peaks at approximately 10.1 billion before declining modestly to 9.9 billion by 2100. This pathway lies within the 95% confidence interval of the medium variant of the UN World Population Prospects 2022. SSP3 describes a world of regional rivalry and stalled human development. High fertility, high mortality, low migration, and stagnant educational attainment (modelled through constant enrolment rates) produce the highest population trajectory of the five pathways: 13.0 billion people by 2100 while global population keeps growing. Sub-Saharan Africa dominates this growth, and the global population retains large low-education segments throughout the century. SSP4 captures a world of increasing within-country stratification. A dual educational structure distinguishes between a highly educated elite and a large segment with limited education (at most lower-secondary). Fertility and mortality assumptions vary by country group, with high-fertility countries experiencing high mortality (as in SSP3), while low-fertility countries follow medium mortality. The global population will reach approximately 11.9 billion by 2100 under this scenario. Across all pathways, the updated WIC2023 projections yield higher populations than WIC2013 in absolute terms, principally due to faster-than-expected mortality decline (particularly child mortality in sub-Saharan Africa) and slower fertility transitions in high-fertility countries.

While the standard SSP population projections go until 2100, extensions to 2300 have been produced to enable long-term demographic and climate dynamics explorations (KC, 2026b). These extended projections use country-specific fertility convergence targets beyond 2100. For the middle-of-the-road SSP2, the global total fertility rate (TFR, in children per woman) is assumed to converge to 1.75 by 2200 across all countries. For SSP1 and SSP5 this convergence is to 1.53, for SSP3 to 1.97 by 2200; note that, unlike the SSP2 value, these are outcomes of applying the low- and high-fertility variants to the education-specific schedules rather than independently imposed global targets. No extensions are currently available for SSP4. Life expectancy at birth is capped globally at 105 years. The results reveal markedly divergent long-run trajectories. Under SSP2, the global population continues its post-2080 decline, reaching 4.2 billion by 2300, with over 22% of the population aged over 80 and only 17% under 20 by that year. Under SSP1 and SSP5, the decline is more severe, with the global population falling to approximately 1 billion by 2300. SSP3, by contrast, projects a peak of over 16 billion people in the 23rd century. Economic projections were not produced beyond 2100 as the uncertainties in model assumptions would be too high.

2.3. Input datasets

2.3.1 Map of administrative units

Disaggregation of population, GDP or asset data recorded at national or subnational level requires a consistent high-resolution map of administrative units. A map was prepared based on OpenStreetMap (2026) national boundaries (including territorial waters), with manual adjustments to remove overlaps or gaps between polygons of countries, and adapt it to the spatial extents available in statistical data sources used in sections 2.3.2–4. In the final map (Fig. 2a), 248 national-level units were defined based on ISO 3166-1 standard (ISO, 2026). The only differences from this standard consist of the omission of Åland Islands (included in Finland) and the uninhabited Antarctica, and inclusion of Kosovo as a separate entry due to much different data availability from Serbia. The vector map was converted into a discrete raster at 30” resolution that uniquely assigns each grid cell to a country.

Similarly, OpenStreetMap was used to generate subnational boundaries, except most of the European countries, which largely follow Eurostat’s nomenclature of territorial units for statistics (NUTS), version 2021, classification (Eurostat, 2020) using a map created for harmonizing European flood impact and exposure data in Paprotny and Mengel (2023). In total, 2652 subnational units were defined for 82 countries (Fig. 2b). The regions are assigned numeric codes based on the ISO country codes and serve as a link between the database of subnational GDP and the map. The vector map was converted into a discrete raster at 30” resolution that uniquely assigns each grid cell to a subnational region. Where available, standardized codes were included in the database of GDP for cross-referencing: ISO 3166-2 ‘country subdivision codes’ and either Eurostat’s NUTS codes or OECD’s territorial classification (OECD, 2026).

https://doi.org/10.5194/egusphere-2026-5045
Preprint. Discussion started: 15 September 2026

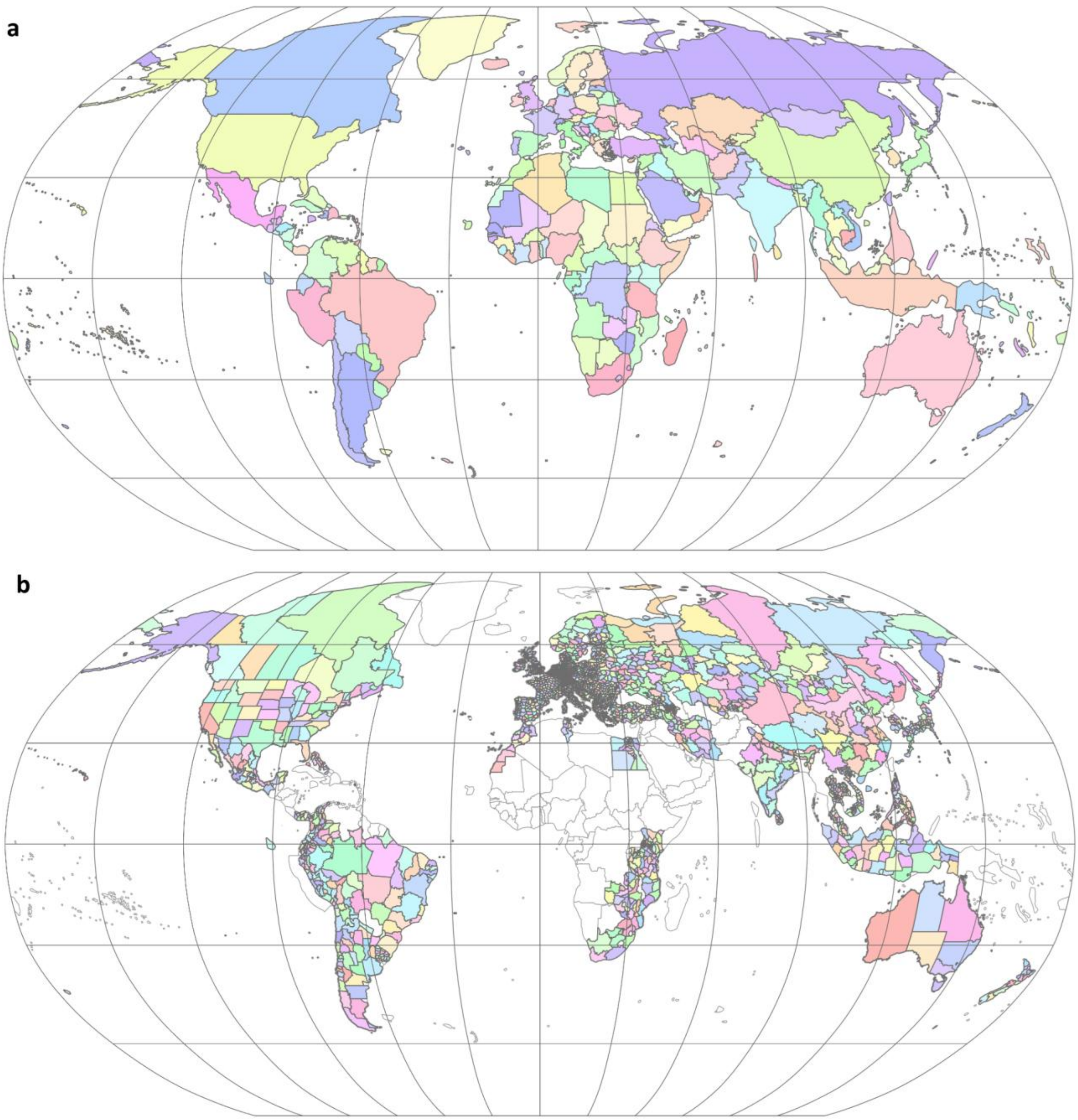

Figure 2. Administrative units at national (a) and subnational (b) level defined in the dataset. Spatial extents include internal and territorial waters. Only the subnational units that are used for GDP disaggregation (section 2.3.3) are shown in (b). Boundaries adapted from OpenStreetMap (2026), except for some European subnational boundaries (Paprotny and Mengel, 2023).

https://doi.org/10.5194/egusphere-2026-5045
Preprint. Discussion started: 15 September 2026

2.3.2 Population

The national-level annual mid-year population timeseries for 1950–2023 were obtained from World Population Prospects: the 2024 (WPP2024) Revision (United Nations 2024), with minor adjustments for consistency with our geographical boundaries (see previous section). Earlier data were obtained from multiple sources. Each country was researched individually to collect the best information publicly available in each case. Where necessary, data were adjusted to a single boundary definition and gap-filled. The exact sources and all data transformations are documented for each territory in Supplementary File 1. For the future, SSP projections (see section 2.2) were adjusted to match the 2020 estimate from WPP2024. The 2024 timestep was interpolated between the latest historical data (2023) and 2025 timestep for the SSP projections. Afterwards, the SSP data was interpolated from 5-yearly timesteps. As the SSP dataset does not cover territories with a population below 100,000 (47 out of 248 defined in this study), future population was gap-filled by extrapolating the historical data with population change in regional aggregates or other countries. SSP regional aggregates were used for minor independent countries, while for small dependent territories the projections for their sovereigns were used. The mapping of our national-level units to SSP countries and regions is shown in Supplementary File 1.

Disaggregation of national-level population was done using available external datasets, as shown in Table 1. The baseline dataset is WorldPop's 'Global2' R2025A, available in 30" resolution for 2015–2030 (Bondarenko et al., 2025a). From 2015-2030, grid-cell population was represented using the WorldPop Global2 gridded population estimates. WorldPop's Global2 datasets provide high-resolution population count surfaces, typically at 3 arc-second resolution, approximately 100 m at the equator, in which administrative census and population projection counts are redistributed to grid cells using Random Forest-based dasymetric modelling. The modelling framework combines population counts with a range of geospatial covariates related to settlement patterns, land cover, infrastructure, accessibility, and other predictors of human population distribution.

Table 1. Gridded population datasets used in the study. * 1975 interpolated from 1970 and 1980 timesteps.

Dataset	Version	Resolution used	Timespan used	Timestep (years)	Reference
HYDE	3.2.1	5' (~9 km)	1850–1975*	10	Klein Goldewijk et al. (2017)
GHS-POP	R2023A	30'' (~1 km)	1975–2015	5	Schiavina et al. (2023); Pesaresi et al. (2024)
WorldPop Global2 *(baseline)*	R2025A	30'' (~1 km)	2015–2025	5	Bondarenko et al. (2025a)
FuturePop	0.2	30'' (~1 km)	2025–2300	5	Bondarenko et al. (2025b)

Before 2015, grid-cell population was extrapolated back in time using 30" resolution population estimates from the GHS-POP dataset that is part of the Global Human Settlement Layer (GHSL). This dataset combines detailed subnational population

https://doi.org/10.5194/egusphere-2026-5045
Preprint. Discussion started: 15 September 2026

counts with remote sensing data on build-up surfaces, achieving high accuracy in estimating spatial population distribution. When comparing with European population grids from 2011 and 2021 censuses (see section 2.5), the average accuracy was very similar to WorldPop, which also used GHSL's built-up surface data. However, we opted to use WorldPop Global2 as baseline due to the availability of SSP-based projections consistent with WorldPop (see below). In any case, all grid-cell population estimates were adjusted by a constant factor to match the total population between the grid and the dataset of national timeseries (Fig. 3). It should be noted that the population is treated as a continuous, rather than a discrete quantity, in all the input grids. The grid-cell population was further extended back to 1850 using the HYDE 3.2.1 dataset. It has a coarser spatial and temporal resolution (~9 km and only 10-year timesteps), but is the only gridded population dataset available for such an extended period. The methodological details of GHS-POP and HYDE are described by Pesaresi et al. (2024) and Klein Goldewijk et al. (2017), respectively.

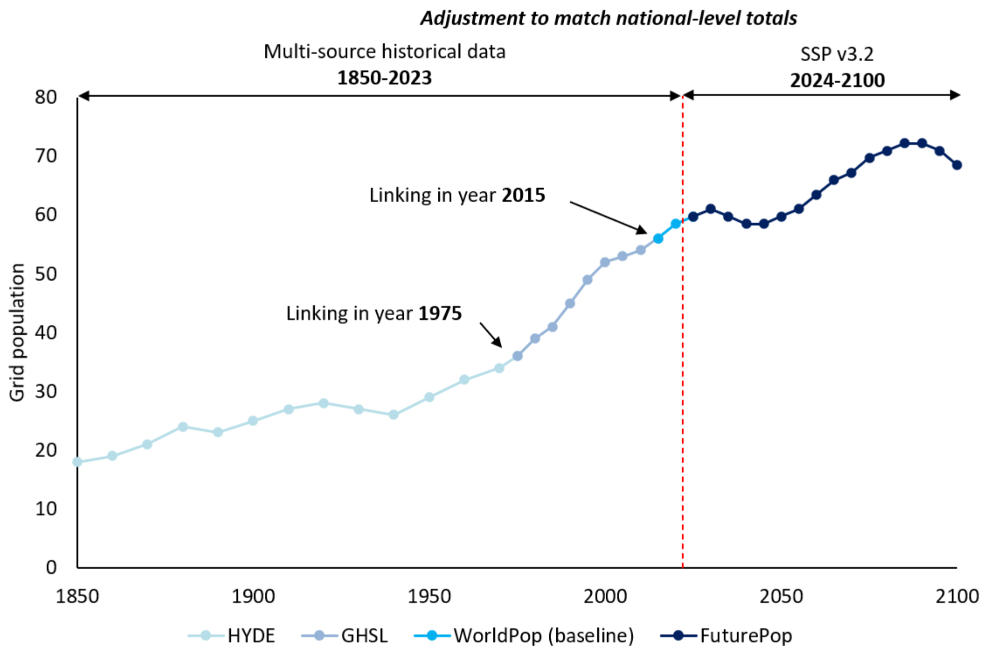

Figure 3. Example of the population merging approach: gridded data are interpolated and harmonized, and then adjusted to national-level total population.

Finally, future projections for the five SSP scenarios were obtained from FuturePop v0.2, an extension of WorldPop Global2 (Bondarenko et al., 2025a). FuturePop v0.2 was produced at 5-year time steps for the period 2025–2100 and subsequently extended to 2300. WorldPop Global2 R2025A (Bondarenko et al., 2025a) provided the spatial baseline: 1 km gridded population distributions, together with subnational population shares, for 2015–2030. For each GADM admin-2 unit, two rates were calculated for each 5-year interval: the fraction of grid cells transitioning to new built-settlement, and the average number of people added per new built-settlement cell. These rates were extrapolated beyond 2025 and combined with a probability-of-transition surface from the Built-Settlement Growth Model (BSGM; Nieves et al., 2020), which ranks non-settlement pixels by their likelihood of becoming settled. Projections then proceeded in 5-year steps from the 2025 baseline. At each step, and within each admin-2 unit, the highest-probability non-settlement pixels were converted to built-settlement, extending urban footprints in line with observed local expansion and infill dynamics. These new urban pixels were populated using the estimated persons-per-new-cell rates, and the resulting distribution was normalised to match SSP national totals exactly while preserving baseline admin-2 population proportions. This produced consistent 1 km projections in which urban areas expand and densify according to historical patterns. Each subsequent step used the projected population from the preceding step as its starting point. Because it follows historical patterns, this method does not explicitly represent the different modes of urbanisation described by the SSP narratives. The approach was first applied to produce 1 km projected population maps for each SSP to 2100, then extended to 2300. In the extension, the SSP4 scenario was not calculated as no input national projections were provided. However, this is not an issue for CMIP7 purposes, as SSP4 is not used in any of the seven emission scenarios that will drive the integrated assessment models (Van Vuuren et al., 2026).

2.3.3 Gross domestic product (GDP) per capita

As for population, all national-level timeseries of GDP per capita were harmonized spatially to a common territory and temporarily to avoid breaks. Data for 2011–2023 were gathered from the National Accounts Main Aggregates Database (United Nations 2025), amended with country-specific sources. Using GDP deflators from the same source, all data were converted to 2017 US dollars and then further converted to purchasing power parities (PPPs). PPPs were mostly taken from revised estimates for 2017 from the International Comparison Programme 2021 dataset (World Bank 2026). The GDP per capita were then extended back to 1850 mostly using the Maddison Project Database 2023 (Bolt and van Zanden, 2025) with the addition of country-specific sources. As for population, the exact sources and all data transformations are documented for each territory in Supplementary File 1. SSP projections until 2100 compliment the dataset and are linked to historical data as for population (see previous section).

Subnational GDP per capita was collected for 82 countries comprising 2652 subnational administrative divisions (Fig. 2b) between 1850 and 2023, representing about 89% of global GDP. Data availability is largely limited to the present century, but some countries have estimates spanning many decades before, even for 1850 (Denmark and Sweden). In many cases, the data was interpolated between available benchmark estimates. All data were, to the extent possible, homogenized to the same administrative boundaries for all years. In many cases of European countries, data at a more aggregated level are available for earlier decades (typically Eurostat's NUTS 2 level), therefore the values at more detailed NUTS 3 level were extrapolated using the appropriate upper-level divisions. All data sources and transformations made to the data are documented for every country in Supplementary File 2. The data were recorded as percentages relative to national GDP per capita. Total GDP and population data, where available, are also recorded in the input dataset for reference, but only the relative GDP per capita is used by the exposure disaggregation (see below). For years where there is no data, the earliest timestep was generally used for

https://doi.org/10.5194/egusphere-2026-5045
Preprint. Discussion started: 15 September 2026

all years prior and the latest data were used for all years afterwards. However, to avoid large distortions in the historical data due to some regions having extremely high GDP per capita related usually to modern fossil fuel production, the relative subnational GDP was not allowed to exceed a 50–200% range in 1850. If a region was above or below this range in the earliest available timesteps, its subnational GDP was interpolated with the limit value, so that it converges with the defined range in 1850.

National-level GDP per capita was multiplied by population (section 2.3.2), disaggregated by subnational administrative units (where available), and then distributed into the grid: 60% proportionally to gridded population and 40% proportionally to built-up area (section 2.3.5). This 60:40 ratio is intended to represent the typical ratio between the contributions of labour and capital inputs to GDP (Arpaia et al., 2009, Piketty and Zucman, 2014, Guerriero, 2019, Office for National Statistics, 2024).

2.3.4 Fixed asset value

Fixed asset value is defined as the stock of all produced non-financial assets that are used repeatedly or continuously in production processes for more than one year, both tangible (e.g. buildings, machinery, transport equipment) and intangible (e.g. software and patents). Inventories, valuables, non-produced assets (e.g. land) and consumer durables are excluded. The value of assets here is their net value, i.e. after deprecation, and inserted into the input database of national-level timeseries as fixed asset-to-GDP ratio. Data on fixed assets are limited and were mostly obtained from Eurostat, OECD or national statistical agencies for most of the developed economies, and supplemented by Penn World Tables v10.01 for 1950–2019 (Feenstra et al. 2015) and Goldsmith (1985) before 1950. As with population and GDP, all country-specific data sources are identified in Supplementary File 1. Still, coverage of data is far from complete, especially before 1950, even using interpolations of available data points.

To gap-fill the fixed asset value, we leverage the observation that fixed asset-to-GDP ratio has a long-term upward trend, attributed by Piketty and Zucman (2014) to the slowdown of productivity and population growth. Using 1458 data points of fixed asset-to-GDP ratios (spaced at least 10 years apart to reduce autocorrelation), we indeed find a positive Spearman's correlation of 0.32 with GDP per capita level in data transformed to a standard normal distribution. We use a bivariate Frank copula to capture the dependency structure and estimate the fixed asset-to-GDP ratio based on each country's GDP per capita (see previous section). The goodness–of-fit of different copula types was measured using a blanket test based on the Cramèr–von Mises statistic (Genest et al., 2009) before choosing the Frank copula. By randomly sampling the copula conditionalized on GDP per capita, the fixed asset-to-GDP ratio was computed for all missing years. If some fixed asset value data was already available for a given country, timeseries from gap-filling were used to extrapolate the earliest and latest available information. The results in the global gap-filled estimates (Fig. 4, light blue line) show an upward trend in fixed asset-to-GDP ratio, except for the period containing the Great Depression and World War II (c. 1930-1950).

https://doi.org/10.5194/egusphere-2026-5045
Preprint. Discussion started: 15 September 2026

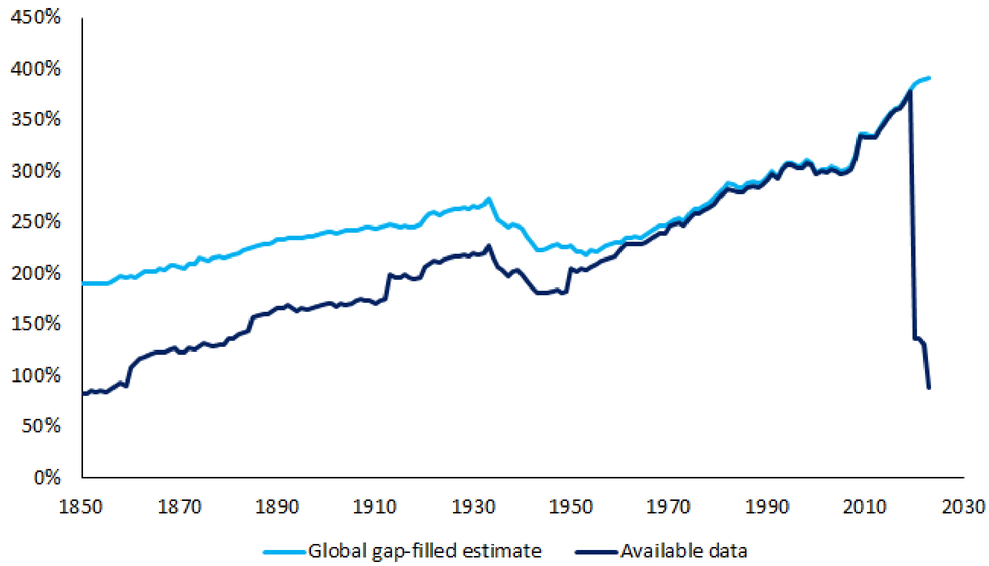

Figure 4. Net fixed asset value in the world relative to global GDP (%), 1850–2023, summation of available data compared with summation of gap-filled estimates.

For the future time period, the fixed asset value was extrapolated from 2023 using the predicted fixed asset-to-GDP per SSP scenario of changes in GDP per capita. Finally, the relative fixed asset value was multiplied by national or subnational (where available) GDP and distributed proportionally to the built-up area (see next section).

2.3.5 Built-up area

The basis for disaggregation of GDP and fixed assets, and for calculating the degree of urbanization was the GHS-BUILT-S dataset (Pesaresi and Politis, 2023) that is part of GHSL. It includes both residential and non-residential surfaces detected from satellite observations and is available in 5-yearly timesteps covering years 1975–2030. As no corresponding datasets are available for earlier or future time periods, the built-up area is extrapolated using the same ratio as population change relative to 1975 (for the past) or 2030 (for the future). However, the built-up surface is not allowed to decline over time in connection to a falling population, as in reality once a surface is built up, it is very rarely restored to a 'natural' state. Also, the future built-up area is capped at the total grid cell area calculated at 30" resolution.

2.4 Degree of urbanization

Using population density and built-up area layers at 30" resolution, we created a grid cell classification according to the Degree of Urbanization (DEGURBA) methodology introduced by European Union/FAO/UN-Habitat/OECD/The World Bank (2021), based on the implementation made by Schiavina et al. (2025). It enables classifying the grid into three main categories (cities, towns, and rural areas), with further into seven more detailed classes (Table 2). The approach involves detection of continuous

https://doi.org/10.5194/egusphere-2026-5045
Preprint. Discussion started: 15 September 2026

clusters of high population density according to Table 2. 4-point connectivity was used for except suburban and rural clusters, where 8-point connectivity was applied. For detecting grid cells belonging to urban centres, we used the optional approach suggested by European Union/FAO/UN-Habitat/OECD/The World Bank (2021) to include cells that are at least 50% built up, to avoid scattering of large urban areas with relatively low population density, e.g. in the United States. Urban centres were additionally smoothed with 3-by-3 conditional majority filtering and gap-filled by removing holes smaller than 15 km^2, as proposed by Schiavina et al. (2025). Uninhabited cells consisting of at least 50% of water were classified as such to distinguish them from very low-density rural areas. The land fraction was computed using GHS-LAND, which combines satellite observations with OpenStreetMap data (Pesaresi and Politis, 2022).

Table 2. Classification of Degree of Urbanization with grid code used in the output dataset. Based on European Union/FAO/UN-Habitat/OECD/The World Bank (2021) and Schiavina et al. (2025).

Grid code	Class	Equivalent settlement type	Cluster population thresholds (persons)	Grid cell density thresholds (persons per km^2)	Additional conditions
	Urban centres	**Cities**			
30	Urban centres	Cities	50,000	1500	Also >50% built-up if below population density threshold
	Urban clusters	**Towns and semi-dense areas**			
23	Dense urban clusters	Dense towns	5000	1500	
22	Semi-dense urban clusters	Semi-dense towns	2500	900	At least 2 km from a dense urban cluster or urban centre
21	Suburban or peri-urban grid cells	Suburban or peri-urban areas	5000	300	
	Rural grid cells	**Rural areas**			
13	Rural clusters	Villages	500	300	
12	Low-density rural grid cells	Dispersed rural areas	-	50	
11	Very low-density rural grid cells	Mostly uninhabited areas	-	-	At least 50% on land
	Water	-			
10	Water	-	-	-	Less than 50% on land and no population

The application of the methodology is not perfectly to the original, as it should be made on a projected, regular 1 km grid. Here, we use a geographical grid of only approximately the same size that varies according to the latitude. We therefore tested whether adjustments of the individual thresholds would be warranted. However, we found the results very similar to the GHSL data classified with the DEGURBA approach and not sensitive to small changes in the thresholds. The comparison between our results and the United Nations World Urbanization Prospects (WUP) 2025 based on GHSL (Schiavina et al., 2025) is shown in section 3.4.

https://doi.org/10.5194/egusphere-2026-5045
Preprint. Discussion started: 15 September 2026

2.5 Validation

We validated the approach of combining multiple population grids with available long-run, high-resolution data. Firstly, we used 1 km population estimates for Spain from HIPGDAC-ES (Goerlich, 2025), covering years 1900–2021 in decadal timesteps. Secondly, we used 1 km population estimates for most European countries covering 2011 and 2021 census rounds (Eurostat, 2025). To extend this data further, we extrapolated the 1 km population cells with municipal-level population (almost 110,000 units) for most European countries based mainly on 1960–2010 data by the European Commission (2013) and assembled by Paprotny and Mengel (2023). Separately, we extrapolated the 1 km population for Austria using harmonized municipal-level (2117 units, incl. districts of Vienna) population since 1869 by Statistik Austria (2026), interpolated to full decades where necessary. The average error per grid cell was analysed at 5' (~9 km) resolution and compared to the HYDE dataset, which was the source of DHF data for previous ISIMIP rounds (Frieler et al., 2024) and is still used in CMIP7 as major input source of the land use forcing dataset LUH3 . Additionally, we made a comparison with the HANZE dataset, which is a high-resolution reconstruction of historical exposure for Europe (Paprotny and Mengel, 2023).

3 Results

3.1 Overview of the dataset

The final dataset consists of eight variables covering the period 1850–2100 in 30" (~1 km) resolution or coarser. Population is available as a total count, density per km^2, and urban only count. GDP total is accompanied by GDP per capita that is evenly distributed across each administrative unit (national and subnational), excluding uninhabited cells. In resolutions coarser than 30", cells shared by multiple administrative units are computed by weighting GDP per capita by population within each contributing unit. This layer is recommended for spatial analyses specifically requiring GDP per capita, as the layer with total GDP is produced by distributing GDP partially by population and partially by built-up surface. Economic variables are complemented by total net fixed asset value.

Table 3. Gridded data layers available in the output dataset.

Variable	Unit	Notes
Population count	Persons	Mid-year estimate
Population density	Persons per km^2	Mid-year estimate
Urban population count	Persons	Mid-year estimate
Gross domestic product (GDP)	2017 US dollar in Purchasing Power Parity	
Gross domestic product per capita	2017 US dollar in Purchasing Power Parity	Distributed evenly or weighted across administrative units
Net fixed asset value	2017 US dollar in Purchasing Power Parity	

Degree of urbanization	Discrete DEGURBA classes	Only 30” resolution
Fraction of urban land	%	Only 1’ or lower resolution
Built-up area	m^2	

In the final dataset at 30” resolution, the degree of urbanization is presented as a discrete classification of grid cells. At coarser resolutions, the results are aggregated by showing the percentage of each grid cell covered by urban land (i.e. either cities or towns and semi-dense areas). Urban population is similarly defined as all persons residing in either cities or towns, and is computed by filtering the 30” grid cells and aggregating the results to the target resolution. Built-up area used to compute the degree of urbanization is also provided in the dataset.

3.2 Long-term population and economic trends, 1850-2100

A global overview of the results shows a relentless increase in population, GDP and fixed asset value since 1850 that will largely continue into the future (Fig. 4). Still, large variations in the growth rates were recorded in the historical period. Even though the temporal resolution of available national-level timeseries is not equal, and for lower-income countries is often much lower than annual particularly before the 1950s, many large global and regional crises (wars, pandemics, famines) are clearly visible in the data. Population growth increased from about 0.5% annually until peaking at above 2% in the 1960s, and is expected to drop to negative before the end of the century in SSP1, SSP2 and SSP5 scenarios. GDP per capita growth oscillated around 1% in the 1850s before accelerating, and has averaged about 2% since the 1950s. A slow decline in the growth rate is generally expected in the future, though after a temporary increase in SSP1 and SSP5. Reduction in the population growth rate means that the global economy also slowed its growth rate since the peak above 4% in the 1950s and 1960s, and will likely continue in the future. Finally, the value of fixed assets relative to GDP doubled since 1850 and should continue to increase in the future if those historical patterns continue in the future.

https://doi.org/10.5194/egusphere-2026-5045
Preprint. Discussion started: 15 September 2026

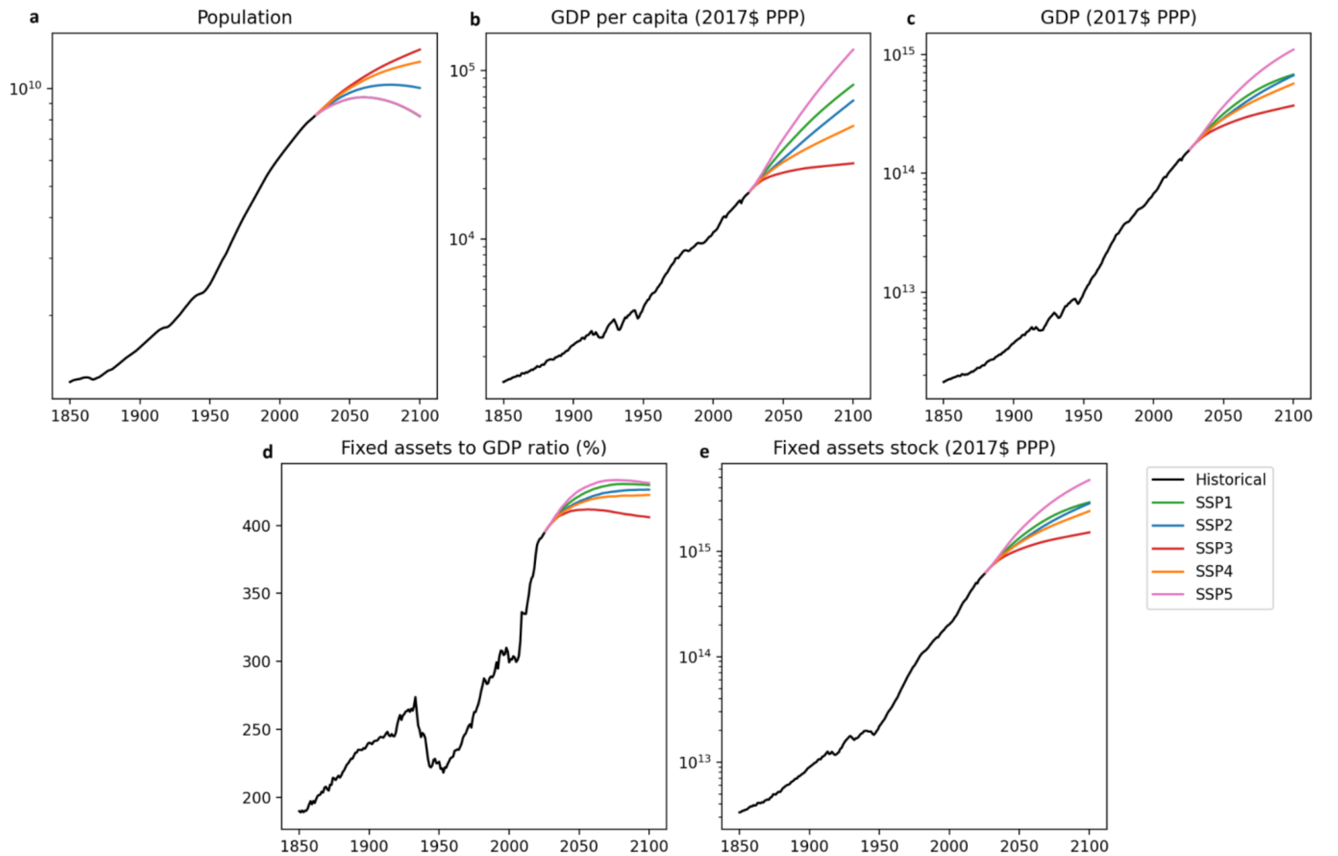

Figure 5. Global trends in main indicators, historical and SSP projections, 1850–2100. The vertical axis is logarithmic except graph (d), which shows values in percentages. The online dataset contains visualizations for all national-level timeseries.

Spatially, there have been large variations between continents and countries. Very few locations experienced population decline between 1850 and 1950, mainly in western Europe and east Asia (Fig. 6a), while in recent decades many parts of Europe and North America recorded a decrease in population (Fig. 6b). In the future, there are large differences between SSP scenarios, but Europe and east Asia is universally expected to decline substantially (Fig. 6c-g). South Asia and the Americas have contrasting futures of growth or decline depending on the scenario. Only Africa, Oceania and most of western Asia is expected to have a larger population in 2100 than at present across all SSP scenarios. GDP change has also been almost entirely upwards, with faster rates of growth in the Americas in particular before 1950 (Fig. 7a) and in Asia afterwards (Fig. 7b). In the future, GDP growth is expected to be the highest in Africa, driven partially by high population growth, and the lowest in more developed regions, particularly Europe and Japan (Fig. 7c-g).

https://doi.org/10.5194/egusphere-2026-5045
Preprint. Discussion started: 15 September 2026

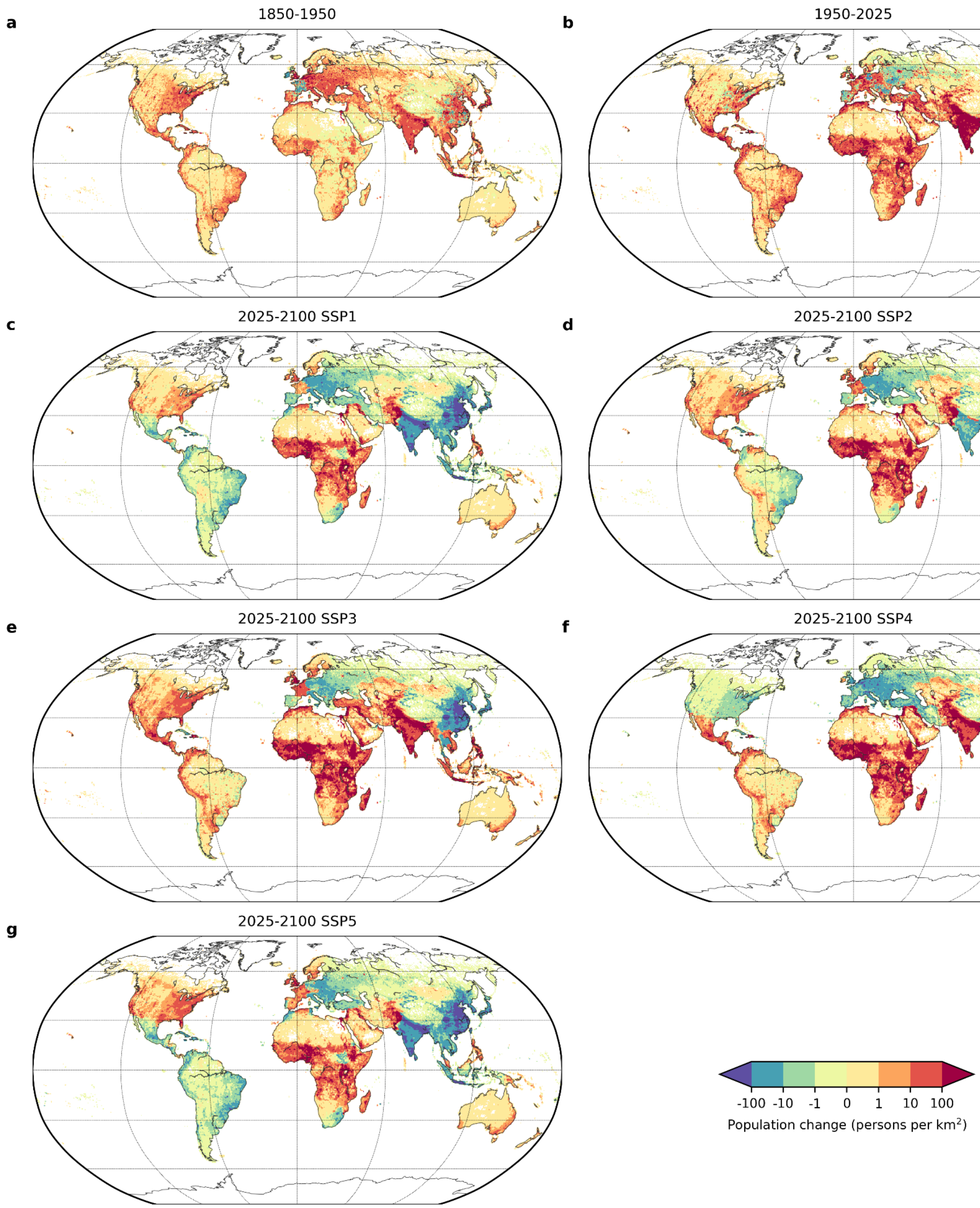

368

369 **Figure 6. Absolute change in population density, 1850–2100, aggregated to 0.5 degree resolution.**

370

https://doi.org/10.5194/egusphere-2026-5045
Preprint. Discussion started: 15 September 2026

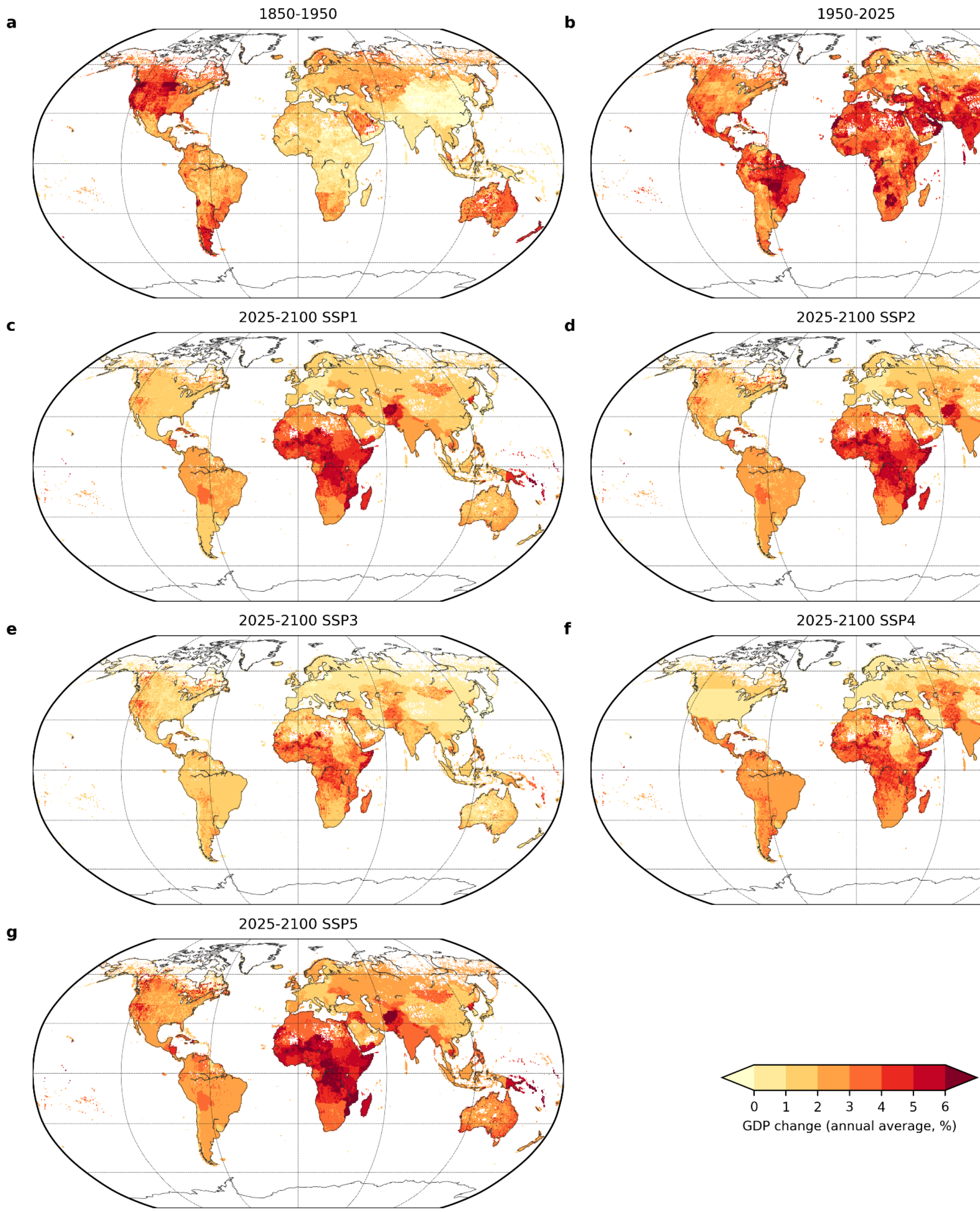

Figure 7. Average annual GDP change, 1850–2100, aggregated to 0.5 degree resolution.

https://doi.org/10.5194/egusphere-2026-5045
Preprint. Discussion started: 15 September 2026

3.3 Trends in the degree of urbanization

The population growth in the past two centuries was concentrated in cities and towns. Since 1850, population in cities of the world increased from only 72 million to 3.7 billion in 2025, contributing to 52% of total population growth in that period. Towns have grown from 361 million to 2.8 billion, while rural areas have only added 13% to global population growth, and are home to 1.7 billion people worldwide. This results in an urbanization rate of 79% in 2025, with urban areas covering 3.7 million km^2, or 2.8% of dry land, which is 11 times more than in 1850. With most of the population already residing in urban areas, future growth in the urbanization rate will be slower, resulting in an urbanization rate of up to 86% (SSP4). Largest growth is expected in Africa, which so far has been the least urbanized continent (Fig. 8).

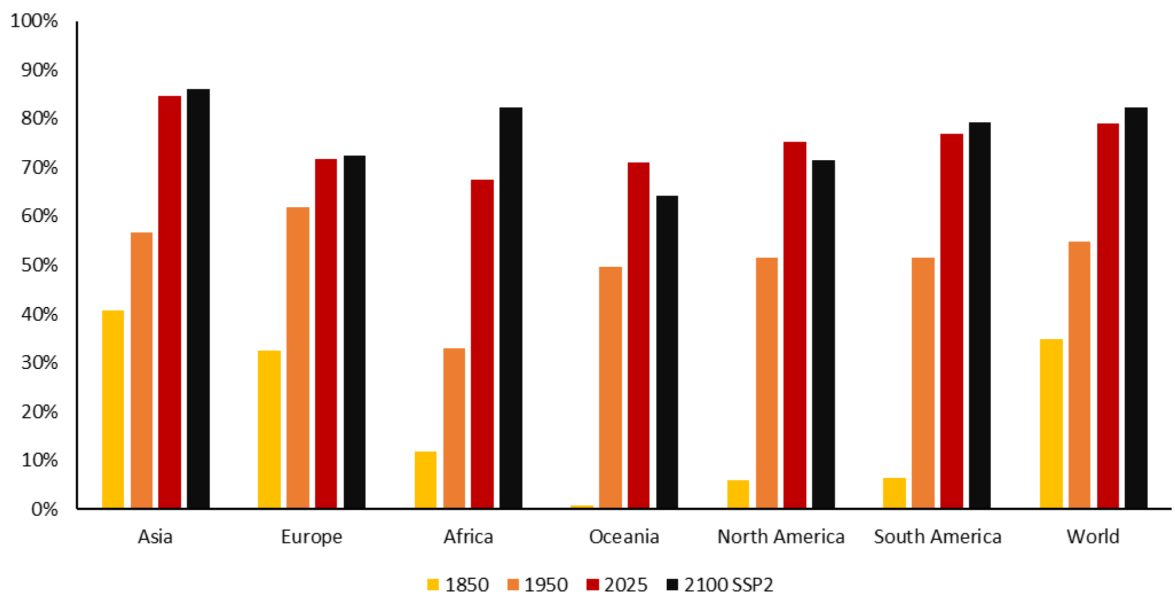

Figure 8. Urbanization rate by continent and globally, 1850–2100.

An extreme example of rapid urbanization is Egypt, where population is concentrated along the Nile delta (Fig. 9), as shown by the population distribution at 30” resolution. We estimate that in 1850 only 6% of Egypt’s population lived in urban centres, marked by red colour in the maps (Fig. 9a). By 2025, the population of cities rose from 0.3 to 83 million, or 69% of total population (Fig. 9c). Further population growth under SSP2 scenario could result in 95% of the population being concentrated predominantly in a single continuous metropolis (Fig. 9d).

https://doi.org/10.5194/egusphere-2026-5045
Preprint. Discussion started: 15 September 2026

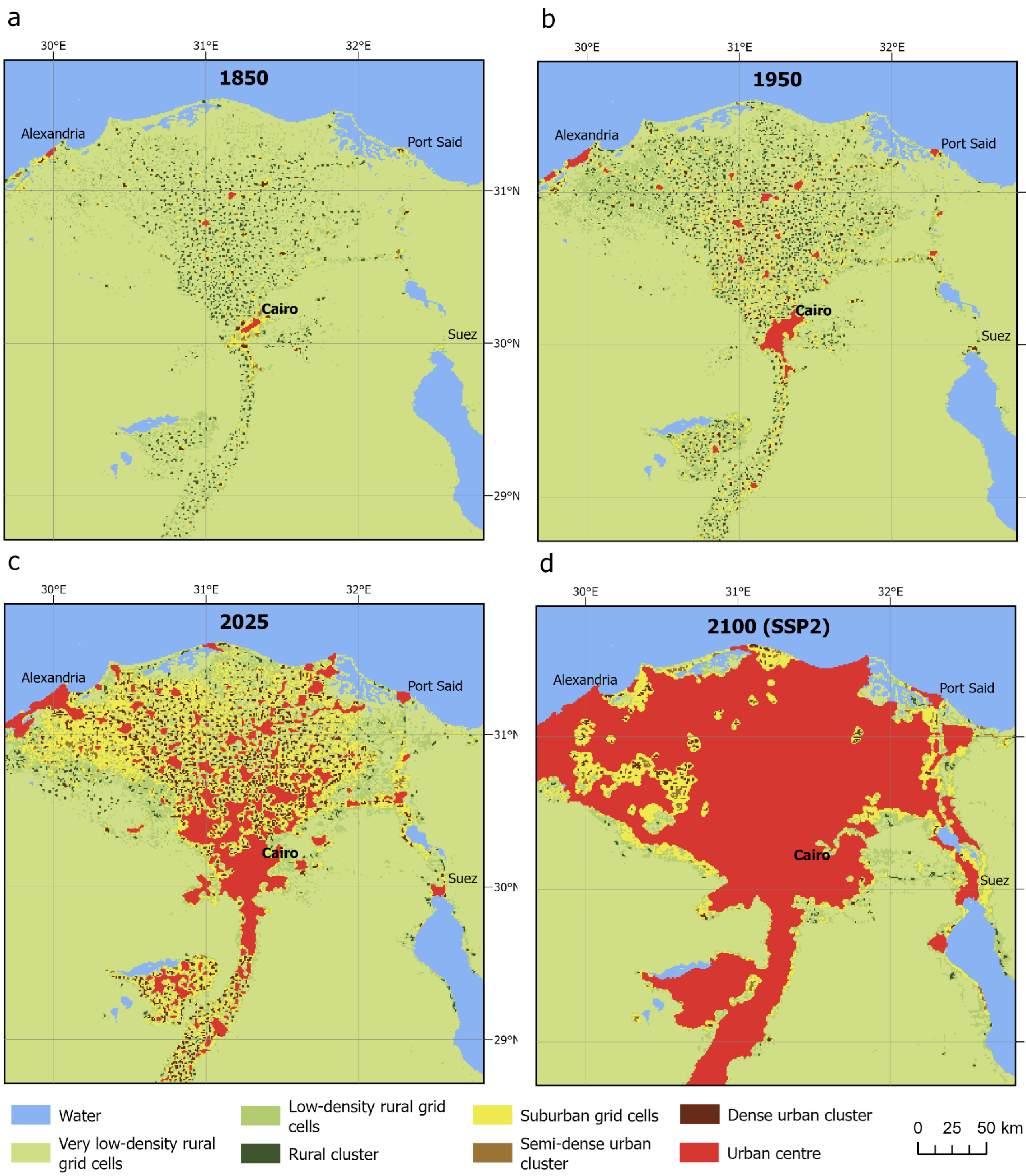

Figure 9. Example application of the Degrees of Urbanization methodology to a 30” (~1 km) population grid: the Nile delta, Egypt, 1850–2100. Cairo and three biggest cities outside the capital region are marked.

https://doi.org/10.5194/egusphere-2026-5045
Preprint. Discussion started: 15 September 2026

3.4 Validation

To validate the approach of merging multiple different gridded datasets and harmonizing them by adjusting to national-level timeseries, we first computed the average error at grid-cell level based on three validation datasets (see section 2.5). Then, we compared the results with the global HYDE 3.2 dataset and pan-European HANZE 2.0. Due to the coarser resolution of HYDE, we evaluated the error at 5' (~9 km) resolution. The results show that in all cases the merged gridded dataset outperformed the HYDE dataset, also achieving similar results on average across Europe compared to HANZE (Fig. 10). The error still increases when moving more into the past, as input population and land use data become increasingly coarser. Some of the error is due to imperfect matches of spatial and temporal reference points between datasets, but still the challenge of exactly estimating population distribution across large domains is clear.

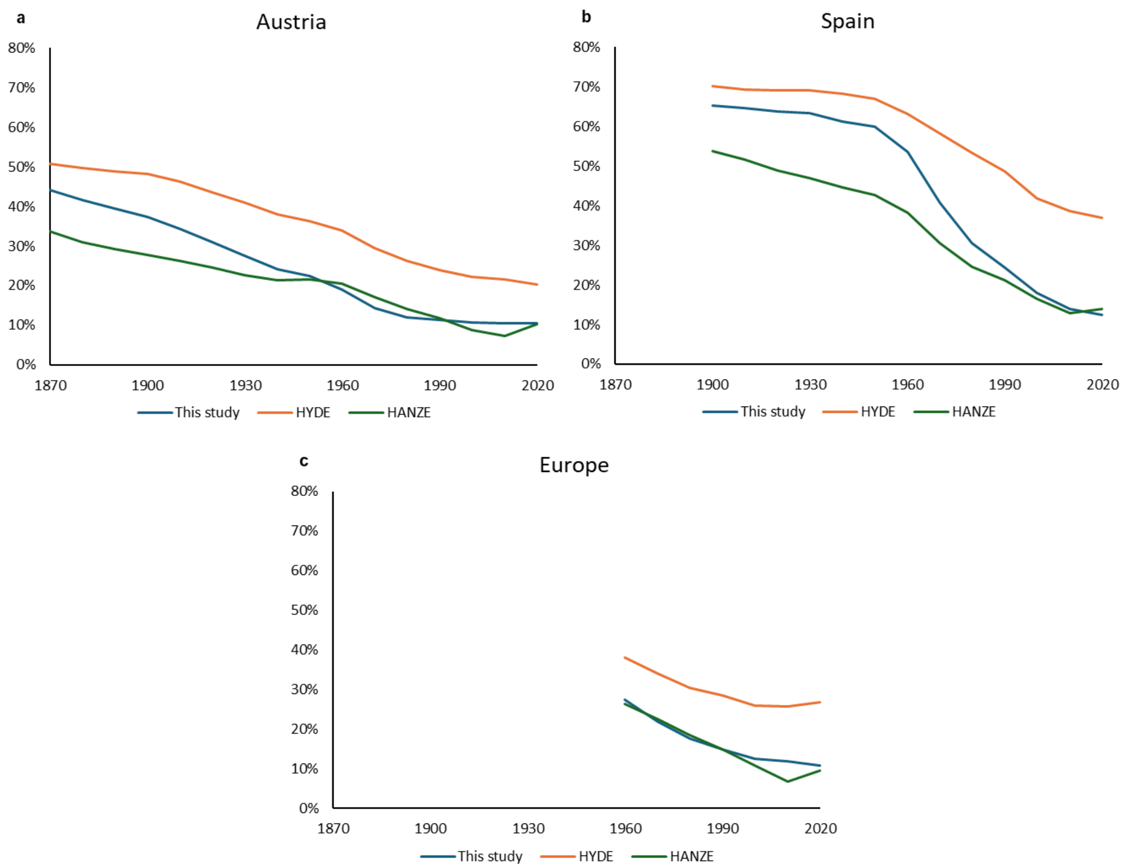

Figure 10. Average error (%) in population distribution at 5' (~9km resolution) from this study for three validation datasets and compared to two other datasets – HYDE (Klein Goldewijk et al., 2017) and HANZE (Paprotny and Mengel, 2023).

https://doi.org/10.5194/egusphere-2026-5045
Preprint. Discussion started: 15 September 2026

We further compare our calculation of the degree of urbanization against other datasets. The primary corresponding dataset is the GHSL-WUP (Schiavina et al., 2025), which follows the same classification and provides very similar urbanization rates globally (Fig. 11). GHSL-WUP has only one future scenario, which corresponds on a conceptual level most closely with SSP2, representing a 'middle-of-the-road' scenario. However, despite the total population of cities and towns being very similar (if slightly lower throughout), GHSL-WUP considers cities as the main source of future demographic growth, while in our results based on FuturePop it is concentrated in towns. This is partially connected to the differences in assumptions about the level of dispersion of urban areas, to which any urban growth model is sensitive in the long temporal perspective. It is notable that the SSP database (IIASA, 2025) provides a vastly different urbanization rate, which is methodological. As was the case with previous World Urbanization Prospects from the United Nations before the 2025 revision, the SSP database uses urbanization defined nationally, resulting in highly heterogeneous and usually underestimated urbanization rates. A similar approach of using national definitions is present in the HYDE dataset. As visible in Fig. 11, there is a strange pattern visible in HYDE: urbanization increases rapidly in the second half of the 19^{th} before stagnating between 1910 and 1950. In our analysis, there is a much more smooth transition since the beginning of the second industrial revolution in the 1870s.

https://doi.org/10.5194/egusphere-2026-5045
Preprint. Discussion started: 15 September 2026

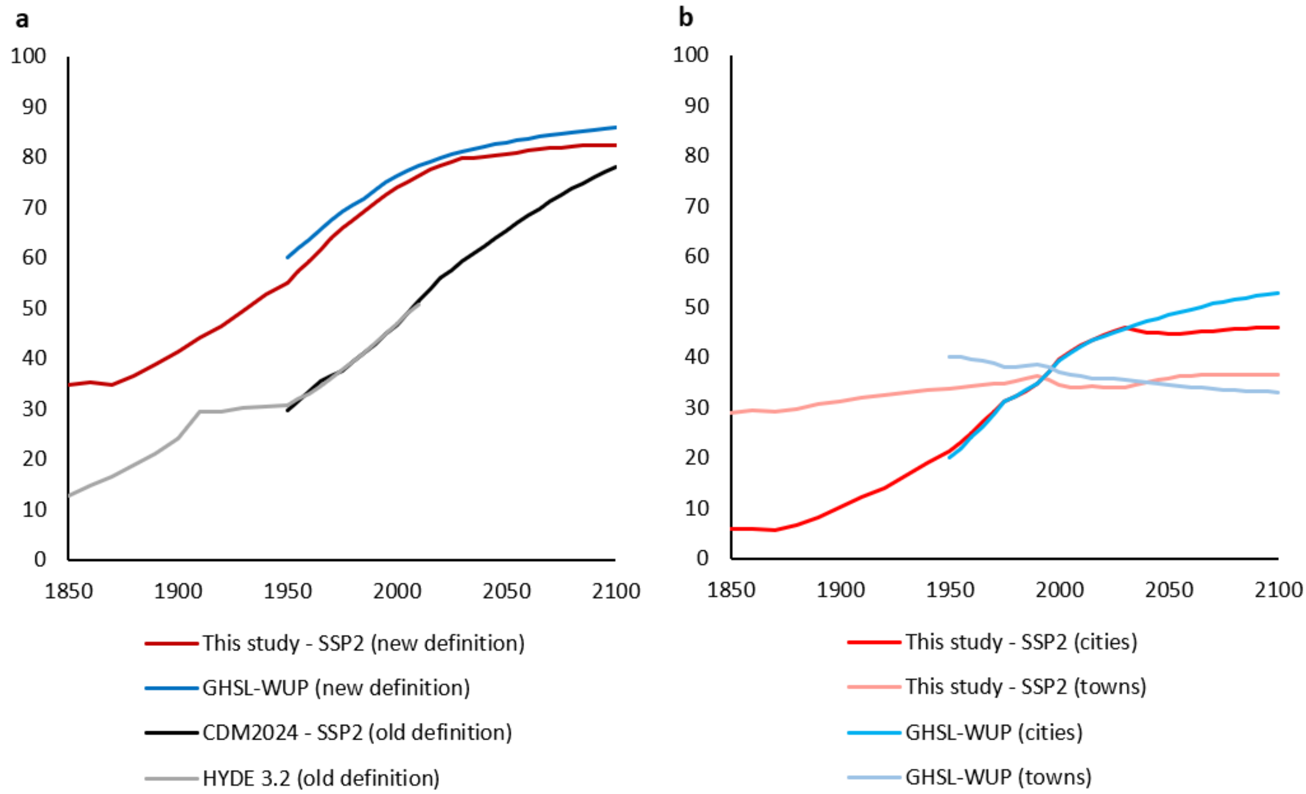

Figure 11. Comparison of urbanization rates (%) globally in this study, GHSL-WUP 2025 (Schiavina et al., 2025), CDM2024 SSP2 scenario (IIASA, 2025) and HYDE 3.2 (Klein Goldewijk et al., 2017) 1850–2100. (a) total urbanization according to the new and old definitions; (b) population in cities or towns.

We also compared national-level urbanization rates between datasets (Fig. 12). Urbanization rates across countries are very similar between our results for 2025 (based on WorldPop) and WUP (based on GHSL), with the largest differences being for very small territories (such as Montserrat, Anguilla, Cook Islands, or Western Sahara). For 1950 and 2100, the dispersion increases, but the correlation remains high.

https://doi.org/10.5194/egusphere-2026-5045
Preprint. Discussion started: 15 September 2026

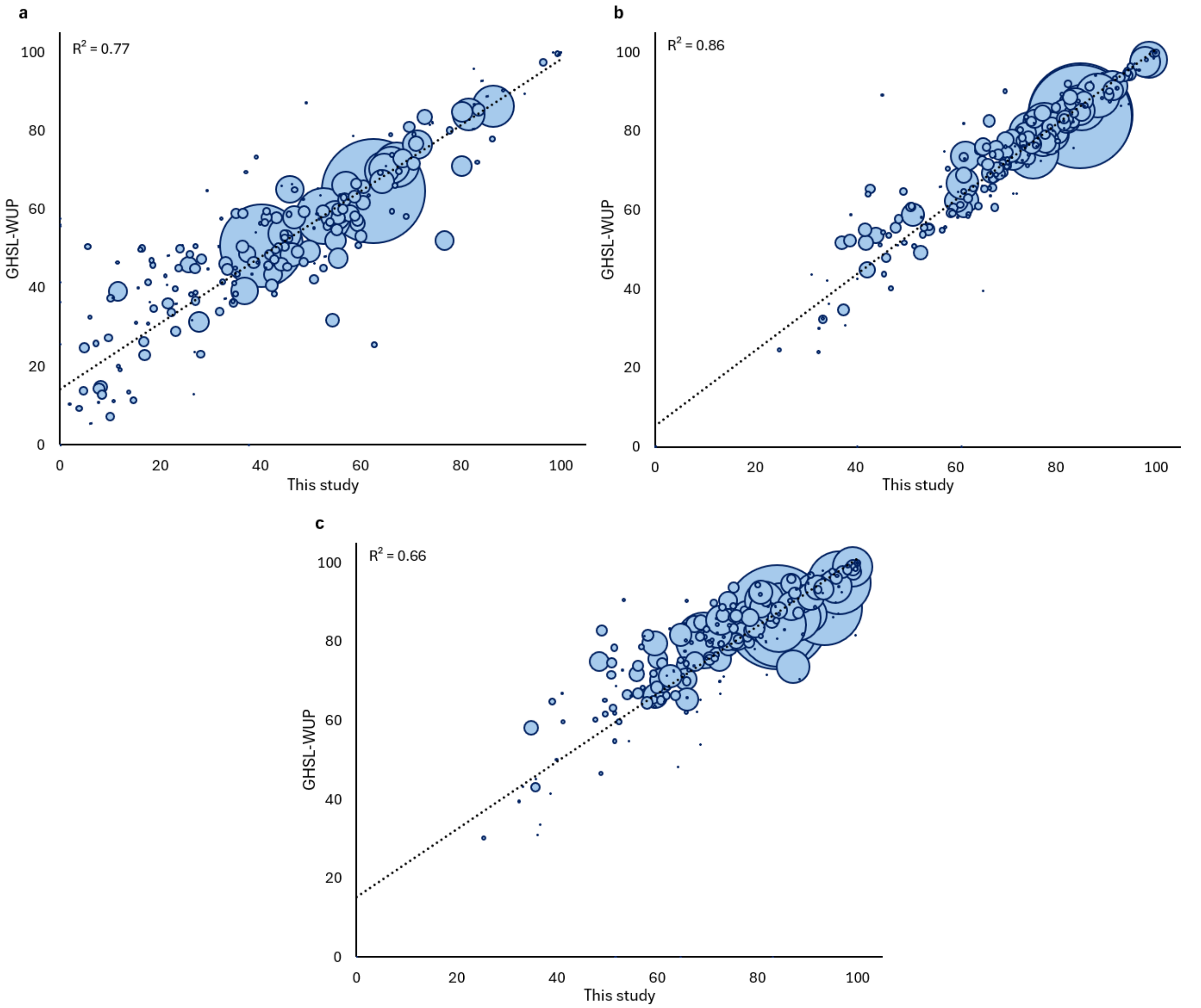

Figure 12. Urbanization rate (cities and towns combined) by country in this study compared with GHSL-WUP 2025 (Schiavina et al., 2025): (a) 1950, (b) 2025, (c) 2100. Area of the bubble is proportional to the total country population in the year analysed.

4 Discussion

4.1 Application of direct human forcing in CMIP7

The most direct need for this data in CMIP7 was expressed for the Fire Modelling Intercomparison Project (FireMIP). Gridded population density information can be used to project changes both in anthropogenic ignitions and in the ability to suppress fires. In future updates to gridded forcings products, including for (anthropogenic) emissions and land use, the possibility to include population changes as a proxy is also enabled by this new dataset, which is specifically useful because of its harmonized

https://doi.org/10.5194/egusphere-2026-5045
Preprint. Discussion started: 15 September 2026

nature, which allows for discerning historical patterns that may be useful for future projections. For instance, internal migration and urbanisation patterns may lead to changes in within-country spatial distributions of emissions for the transportation and residential and commercial emissions. As CMIP7 is evolving (Dunne et al. 2025), this data may be used in many more MIPs under CMIP7 (World Climate Research Programme, 2026).

For CMIP7, we provided population density data in two resolutions (0.25° and 0.5°), which are publicly accessible through the Earth System Grid Federation. Historical data (1850-2025) are stored on ESGF nodes with the identifier "PIK-CMIP-1-0-1". Future projections until 2100, including historical data from 2022 for convenience of modelling groups, were assigned to seven emission scenarios (Van Vuuren et al., 2026) and have the identifier "PIK-*scenario*-1-0-0", where *scenario* is an acronym defined as follows:

- h - High (based on SSP3)
- hl - High-to-Low (based on SSP5)
- m - Medium (based on SSP2)
- ml - Medium-to-Low (based on SSP2)
- l - Low (based on SSP2)
- ln - Low-to-Negative (based on SSP2)
- vl - Very Low (based on SSP1)

Extensions of population density to 2101-2300 are split into two files (2101-2200 and 2201-2300), and can be found with the identifier "PIK-*scenario*-ext-1-0-0", where *scenario* is an acronym as in the list above.

4.2 Application of direct human forcing in ISIMIP

The impact community strongly relies on GDP and population data seamlessly covering the time period 1850-2100. Depending on the purpose these dataset are required at different resolutions and with varying temporal coverage and in case of population data also urban and rural population shares. Within ISIMIP, process based impact models from various sectors (e.g. water, biomes, health, fisheries and marine ecosystems, and energy) make use of population and GDP data at their standard 0.5° resolution to account for the human interventions and activities shaping critical impact variables (Frieler et al., 2024, 2026). In general, the population and GDP forcings are incorporated to resolve economic activity, resource demand, anthropogenic stressors, and vulnerabilities. ISIMIP4a aims for a simulation of historical impacts to allow for model evaluation and impact attribution making use of forcing data, which is as close to observations as possible. This highlights the need for an approach allowing to combine the best available historical data sources for both the early and the recent past. At the same time, future projections dynamically accounting for socio-economic changes (ISIMIP4b group III) require population and GDP projections consistent with the latest SSP scenarios seamlessly harmonized with historical data both at the national and the grid level, to avoid inconsistencies with the historical baseline at all scales. Besides the use of GDP and Population data as direct human forcing for impact models, these datasets are key to derive direct socio-economic impacts such as displacements, damage, exposed population or fatalities from extreme weather events provided as ISIMIP derived output (Lange et al., 2020, Thiery et al., 2021, Schewe et al., 2026). For damage assessments usually an estimation of exposed assets is required to calculate damages based on the hazard intensity and the asset vulnerability. This comes with the need for high resolution estimates of build-up assets. While previous studies worked with resolutions of 150" to 300" (Sauer et al. 2021, Stalhandske et al. 2024), the presented dataset will allow for historical impact attribution and future risk assessments at resolutions up to 30". Upcoming developments entail an improvement of the impact model resolution to 0.1° for selected sectors starting with simulations for Europe (ISIMIP Europe). These enhancements come with the need for better resolved direct human forcing data including population and GDP and will benefit from the flexible approach to generate these datasets at various resolutions. In 2025, the macro-economic multimodel intercomparison project on indirect economic impacts of extreme events (macroMIP) was initiated in close collaboration with ISIMIP, to compare indirect impacts of extreme events in macro-economic models to improve the understanding of the mechanisms of indirect impacts. MacroMIP also strongly relies on population and GDP to simulate the economic development along given GDP baselines. The data for population, GDP and fixed asset value at various resolutions was produced for ISIMIP4 for the historical (4a) and future (4b) scenarios and will become publicly available soon (ISIMIP, 2026b).

4.3 Other applications

The dataset was designed for flexibility in applications across spatial scales and topics. Apart from the application to CMIP and ISIMIP, the dataset in its current (Paprotny, 2025b) or preliminary versions (Paprotny, 2025a) was applied in several studies already. For example, in the "Compound extremes attribution of climate change: towards an operational service" (COMPASS) project (Vertegaal et al., 2026, Paprotny et al., 2025), our estimates of population, GDP, and asset value was used to reassess damages from high wind speeds generated by extra-tropical cyclone Xynthia in 2010 and attribute them to changes in exposure (Compass, 2026). Serres et al. (2025) used our gridded population data for attribution of the historical spread of tropical mosquito-borne viruses in Europe, and projection of the future risk of tropical diseases under climate change in Europe. Pietroiusti et al. (2026) also used our gridded population data to analyse past and future changes in lifetime exposure of people to extreme fire weather at different spatial scales (Portugal and Europe). In another example, Luderer et al. (2026) utilized our urban population and GDP data to develop a spatially explicit framework to downscale future global emissions pathways to urban areas.

One important application for the dataset would be the emerging field of socio-hydrology, which looks into the dynamic interactions between society and hydrological risks (Barendrecht et al., 2017). Changes in floodplain population, urbanization rates or GDP can be analysed to search for existence of the "levee effect", wherein settlement growth close to rivers or coasts is encouraged by perceived safety behind flood defences, or the "adaptation effect", wherein exposure growth is reduced by disinclination to live or invest in floodplains due to experience of past flood disasters (Di Baldassare et al., 2015). Similarly, the "reservoir effect" pertains to population growth encouraged by enhanced water supply through reservoir storage, potentially leading to unsustainable water usage (Di Baldassare et al., 2018). High-resolution DHF could be used to detect those effects at different spatial scales, and quantify practical socio-hydrological models, also under future climate change conditions

https://doi.org/10.5194/egusphere-2026-5045
Preprint. Discussion started: 15 September 2026

(Schoppa et al., 2024). We will use the global exposure dataset in this context within the framework of the ongoing "Flood Adaptation under Climate Change with the European Socio-Hydrological Model" (EuroSoHo) project (ttps://eurosoho.eu/, last access: 25 May 2026).

4.4 Uncertainties and limitations

None of the datasets contributing to this DHF dataset is completely error-free and accurate. The validation for both total and urban populations indicates room for future improvements. Some aspects could not be validated due to a lack of comparable data. In particular, GDP is an estimate of annual production and consumption that is already troublesome to compute at the level of subnational units, let alone in higher spatial resolutions. More detailed disaggregation could be possible with high-resolution land use data, but that would also require long-run historical and projected data on GDP by economic sectors (agriculture, fishing, mining, industry, etc.). Population projections from FuturePop have the limitation of assuming constant relative distribution of population at the subnational administrative levels, which could underestimate urbanization in some countries. Still, this conservative approach helps to avoid major distortions that were visible in previous studies. For instance, Steinhausen et al. (2022) noted that the regional population change patterns for Europe in gridded projections by Murakami and Yamagata (2019) are very different from regional projections from Eurostat. They also note the high concentration of future population growth in European city cores in Jones and O'Neill (2016) in contrast to extensive suburbanization observed in recent decades.

Long development cycles of CMIP, ISIMIP or other major climate-change research projects mean that over time the forcing datasets lose their timeliness (Naik et al., 2025). While population distribution changes slowly over time, except for major displacements related to armed conflicts or disasters, economic growth varies to a much higher degree. Consequently, the algorithm behind this dataset includes an option to leverage data with higher frequency such as the half-yearly updates of the World Economic Outlook (WEO) by the International Monetary Fund (2026), containing short-term GDP projections for up to 5 years ahead. If the option is enabled, the code will replace SSP projections with the WEO data and then slowly converge with the SSP projection by year 2100. Similarly, GHSL and UN population projections can be used up to 2030 with convergence to SSP trajectories by 2100. By default, this extra harmonization step is not enabled for consistency with the SSPs, but might be useful for researchers requiring more up-to-date information for impact modelling.

The global data presented here by necessity generalize many processes occurring in more local scales and do not cover all aspects covered by SSP projections (e.g. population by sex and age, education levels) or needed as DHF (e.g. non-urban land use, detailed agricultural variables or water management-related information). Other studies provide more localized downscaling of projections at continental or national scales (e.g. Winkler et al., 2026, Bonatz et al., 2026), which could also be useful for analyses at smaller spatial scales.

https://doi.org/10.5194/egusphere-2026-5045
Preprint. Discussion started: 15 September 2026

5 Conclusions

This study resulted in a new framework for combining multiple datasets into a coherent forcing dataset for use in earth system and impact modelling spanning the historical and future time periods. The dataset was designed to be a flexible and scalable solution for consistent application of direct human forcing across the current cycle of climate change research. With the code and input data accessible online (Paprotny, 2025b), the users can generate the dataset in any resolution that is a multiplier of 30” (~1 km). The full dataset in the highest resolution was not provided only due to the large size of all files. A subset of data generated specifically for CMIP7 (1850–2300) and ISIMIP4 (1850–2100) is fully accessible online (see “Code and data availability”). Research will continue to expand the range of variables in the data and improve the quality of both historical estimates and future projections.

Code and data availability

The code to produce the DHF dataset presented in this study, together with the necessary input data, is provided on Zenodo: https://zenodo.org/records/17572467 (Paprotny, 2025b). Only a selection of data produced in the study is accessible on Zenodo as the data at 30” resolution for all variables and timesteps approaches 1 TB in size: https://zenodo.org/records/17572467 (Paprotny, 2025b). The population density forcing data used in CMIP7 (0.25 and 0.5 degree resolution, 1850–2300) are available on ESGF - for a list of applicable identifiers, see https://input4mips-cvs.readthedocs.io/en/latest/dataset-overviews/population/ (Paprotny and Hawker, 2026). A copy of the CMIP7 data is also stored on Zenodo: https://zenodo.org/records/19353707 (Paprotny, 2026). National-level SSP scenarios are available from IIASA: https://ssp.apps.ece.iiasa.ac.at/documentation/basic-drivers (IIASA, 2025). The 2025-based scenarios used here are archived at https://doi.org/10.5281/zenodo.21738149 (KC, 2026a). Population count, GDP and fixed asset value used in ISIMIP4 (1 arc min, 5 arc min, 0.1, 0.25 and 0.5 degree resolutions, 1850–2100) will become available on the ISIMIP Repository soon: https://data.isimip.org/ (ISIMIP, 2026b).

Author contributions

DP: Conceptualization, Data curation, Formal analysis, Methodology, Software, Validation, Visualization, Writing (original draft preparation). MB, EN, AJT: Data curation. IS, JSK: Conceptualization, Methodology, Writing (original draft preparation). KF: Conceptualization, Methodology. SKC, RD: Data curation, Writing (original draft preparation). LH: Methodology, Writing (original draft preparation). All authors: Writing (review and editing).

Competing interests

We declare no conflicts of interest.

Disclaimer

We use the term 'country' widely for brevity, and also use a specific representation of national and subnational boundaries that does not represent a particular point in time but is done for the practical purpose of harmonizing various statistical datasets. All this is done without prejudice as to the status of any geographical entity or territory.

Funded by the European Union (see "Financial support" section). Views and opinions expressed are however those of the author(s) only and do not necessarily reflect those of the European Union or the European Research Council. Neither the European Union nor the granting authority can be held responsible for them.

Acknowledgements

We would like to thank Doris Vertegaal for her help in testing the model code, and the CMIP Climate Forcings Task Team for their support in preparation and publishing the population forcing data.

Financial support

DP was supported by the European Union's HORIZON research and innovation action programme through project "Compound extremes attribution of climate change: towards an operational service" (COMPASS), grant no. 101135481, and additionally through ERC Starting Grant "Flood Adaptation under Climate Change with the European Socio-Hydrological Model" (EuroSoHo), grant no. 101218797.

References

Arpaia, A., Pérez, E., and Pichelmann, K.: Understanding labour income share dynamics in Europe, Economic Papers, 379, European Commission, Directorate-General for Economic and Financial Affairs, https://ec.europa.eu/economy_finance/publications/pages/publication15147_en.pdf, 2009.

Barendrecht, M., Viglione, A., and Blöschl, G.: A dynamic framework for flood risk. Water Secur., 1, 3–11. https://doi.org/10.1016/j.wasec.2017.02.001, 2017.

Bolt, J., and van Zanden, J. L: Maddison style estimates of the evolution of the world economy: A new 2023 update. J. Econ. Surv., 39, 631–671, https://doi.org/10.1111/joes.12618, 2025.

Bonatz, H., Nikoletopoulos, T., & Vafeidis, A. T.: Updated spatial population projections for the EU and the UK under the shared socioeconomic pathways provide new insights for climate impact assessments, Earth's Future, 14, e2025EF006504, https://doi.org/10.1029/2025EF006504, 2026.

Bondarenko M., Priyatikanto R., Tejedor-Garavito N., Zhang W., McKeen T., Cunningham A., Woods T., Hilton J., Cihan D., Nosatiuk B., Brinkhoff T., Tatem A., and Sorichetta A.: The spatial distribution of population in 2015-2030 at a resolution

https://doi.org/10.5194/egusphere-2026-5045
Preprint. Discussion started: 15 September 2026

of 30 arc (approximately 1km at the equator) R2025A version v1. [dataset], https://doi.org/10.5258/SOTON/WP00845, 2025a.

Bondarenko M., Tejedor-Garavito N., Priyatikanto R., Zhang W., Fang W., Nosatiuk B., Gaskell J., McKeen T., Noi E., Hilton J., Butterick J., Hawker L., and Tatem A. J..: Global 1km-grid population projections for 2025-2100 consistent with the Shared Socioeconomic Pathways 3.2 national population projections, version 0.2" 2025 [dataset], https://doi.org/10.5258/SOTON/WP00849, 2025b.

Compass: France. Extra-tropical cyclone 'Xynthia' in 2010, https://uc.compass-climate.eu/stories/france, (last access: 28 May 2026), 2026.

Dellink, R., Chateau, J., Lanzi, E., and Magné, B.: Long-term economic growth projections in the Shared Socioeconomic Pathways, Global Environ. Change, 42, 200–214, https://doi.org/10.1016/j.gloenvcha.2015.06.004, 2017.

Di Baldassarre, G., Viglione, A., Carr, G., Kuil, L., Yan, K., Brandimarte, L., and Blöschl, G.: Debates-Perspectives on socio-hydrology: Capturing feedbacks between physical and social processes. Water Resour. Res., 51(6), 4770–4781, https://doi.org/10.1002/2014WR016416, 2015.

Di Baldassarre, G., Wanders, N., AghaKouchak, A., Kuil, L., Rangecroft, S., Veldkamp T. I. E., Garcia, M., van Oel, P. R., Breinl, K., and van Loon, A. F.: Water shortages worsened by reservoir effects. Nat. Sustain., 1 (11), 617–622, https://doi.org/10.1038/s41893-018-0159-0, 2018.

Dunne, J. P., Hewitt, H. T., Arblaster, J. M., Bonou, F., Boucher, O., Cavazos, T., Dingley, B., Durack, P. J., Hassler, B., Juckes, M., Miyakawa, T., Mizielinski, M., Naik, V., Nicholls, Z., O'Rourke, E., Pincus, R., Sanderson, B. M., Simpson, I. R., and Taylor, K. E.: An evolving Coupled Model Intercomparison Project phase 7 (CMIP7) and Fast Track in support of future climate assessment, Geosci. Model Dev., 18, 6671–6700, https://doi.org/10.5194/gmd-18-6671-2025, 2025.

Durack, P. J., and Nicholls, Z.: input4MIPs Controlled Vocabularies (CVs) [software], https://doi.org/10.5281/zenodo.20032720, 2026.

Durack, P. J., Naik, V., Nicholls, Z., O'Rourke, E., Turner, B., Buontempo, C., Brookshaw, A., Goddard, C., MacIntosh, C., Hewitt, H., and Dunne, J.: Earth System Forcing for CMIP7 and Beyond. Bull. Amer. Meteor. Soc., 106, E1580–E1588, https://doi.org/10.1175/BAMS-D-25-0119.1, 2025b.

Durack, P. J., Taylor, K. E., Gleckler, P. J., Meehl, G. A., Lawrence, B. N., Covey, C., Stouffer, R. J., Levavasseur, G., Ben-Nasser, A., Denvil, S., Stockhause, M., Gregory, J. M., Juckes, M., Ames, S. K., Antonio, F., Bader, D. C., Dunne, J. P., Ellis, D., Eyring, V., Fiore, S. L., Joussaume, S., Kershaw, P., Lamarque, J.-F., Lautenschlager, M., Lee, J., Mauzey, C. F., Mizielinski, M., Nassisi, P., Nuzzo, A., O'Rourke, E., Painter, J., Potter, G. L., Rodriguez, S., and Williams, D. N.: The Coupled Model Intercomparison Project (CMIP): Reviewing project history, evolution, infrastructure and implementation, EGUsphere [preprint], https://doi.org/10.5194/egusphere-2024-3729, 2025a.

European Commission: Population data collection for European local administrative units from 1960 onwards – Final report, Directorate-General for Regional and Urban Policy and Spatial Foresight GmbH, Publications Office of the European Union, Luxembourg, https://doi.org/10.2776/96964, 2013.

https://doi.org/10.5194/egusphere-2026-5045
Preprint. Discussion started: 15 September 2026

European Union/FAO/UN-Habitat/OECD/The World Bank: Applying the Degree of Urbanisation. A methodological manual to define cities, towns and rural areas for international comparisons: 2021 edition, Publications Office of the European Union, Luxembourg, https://doi.org/10.2785/706535, 2021.

Eurostat: Population grids, https://ec.europa.eu/eurostat/web/gisco/geodata/population-distribution/population-grids, (last access: 26 May 2026), 2025.

Eurostat: Statistical regions in the European Union and partner countries — NUTS and statistical regions 2021, Publications Office of the European Union, Luxembourg, https://doi.org/10.2785/850262, 2020.

Frieler, K., Lange, S., Schewe, J., Mengel, M., Treu, S., Otto, C., Volkholz, J., Reyer, C. P. O., Heinicke, S., Jones, C., Blanchard, J. L., Harrison, C. S., Petrik, C. M., Eddy, T. D., Ortega-Cisneros, K., Novaglio, C., Heneghan, R., Tittensor, D. P., Maury, O., Büchner, M., Vogt, T., Quesada-Chacón, D., Emanuel, K., Lee, C.-Y., Camargo, S. J., Hamester, L., Jägermeyr, J., Rabin, S., Klar, J., Vega del Valle, I. D., Novak, L., Sauer, I. J., Lasslop, G., Chadburn, S., Burke, E., Gallego-Sala, A., Smith, N., Chang, J., Hantson, S., Burton, C., Gädeke, A., Li, F., Gosling, S. N., Müller Schmied, H., Hattermann, F., Hickler, T., Marcé, R., Pierson, D., Thiery, W., Mercado-Bettín, D., Ladwig, R., Ayala, A. I., Forrest, M., Bechtold, M., Reinecke, R., de Graaf, I., Kaplan, J. O., Koch, A., Lengaigne, M., Kumar, R., and Strokal, M.: Scenario set-up and the new CMIP6-based climate-related forcings provided within the third round of the Inter-Sectoral Model Intercomparison Project (ISIMIP3b, group I and II), Geosci. Model Dev., 19, 4095–4135, https://doi.org/10.5194/gmd-19-4095-2026, 2026.

Frieler, K., Volkholz, J., Lange, S., Schewe, J., Mengel, M., del Rocío Rivas López, M., Otto, C., Reyer, C. P. O., Karger, D. N., Malle, J. T., Treu, S., Menz, C., Blanchard, J. L., Harrison, C. S., Petrik, C. M., Eddy, T. D., Ortega-Cisneros, K., Novaglio, C., Rousseau, Y., Watson, R. A., Stock, C., Liu, X., Heneghan, R., Tittensor, D., Maury, O., Büchner, M., Vogt, T., Wang, T., Sun, F., Sauer, I. J., Koch, J., Vanderkelen, I., Jägermeyr, J., Müller, C., Rabin, S., Klar, J., Vega del Valle, I. D., Lasslop, G., Chadburn, S., Burke, E., Gallego-Sala, A., Smith, N., Chang, J., Hantson, S., Burton, C., Gädeke, A., Li, F., Gosling, S. N., Müller Schmied, H., Hattermann, F., Wang, J., Yao, F., Hickler, T., Marcé, R., Pierson, D., Thiery, W., Mercado-Bettín, D., Ladwig, R., Ayala-Zamora, A. I., Forrest, M., and Bechtold, M.: Scenario setup and forcing data for impact model evaluation and impact attribution within the third round of the Inter-Sectoral Impact Model Intercomparison Project (ISIMIP3a), Geosci. Model Dev., 17, 1–51, https://doi.org/10.5194/gmd-17-1-2024, 2024.

Goerlich, F. J.: HIPGDAC-ES: historical population grid data compilation for Spain (1900–2021). Sci. Data, 12, 280, https://doi.org/10.1038/s41597-025-04533-8, 2025.

Guerriero, M.: The Labor Share of Income around the World: Evidence from a Panel Dataset. ADBI Working Paper Series, 920, Asian Development Bank Institute, https://www.adb.org/sites/default/files/publication/484346/adbi-wp920.pdf, 2019.

IIASA: SSP Scenario Explorer 3.2.0, Release May 2025, https://data.ece.iiasa.ac.at/ssp/#/workspaces, (last access: 25 May 2026), 2025.

International Monetary Fund: World Economic Outlook (WEO), https://data.imf.org/en/datasets/IMF.RES:WEO, (last access: 29 May 2026), 2026.

ISIMIP: Inter-Sectoral Impact Model Intercomparison Project: https://www.isimip.org, (last access: 25 May 2026), 2026a.

ISIMIP: ISIMIP Repository, https://data.isimip.org/, (last access: 23 July 2026), 2026b.
ISO: ISO 3166 Country Codes, https://www.iso.org/iso-3166-country-codes.html, (last access: 25 May 2026), 2026.
Jones, B., O'Neill, B. C.: Spatially explicit global population scenarios consistent with the Shared Socioeconomic Pathways. Environ. Res. Lett., 11, 084003, https://doi.org/10.1088/1748-9326/11/8/084003, 2016.
KC, S. and Lutz, W.: The human core of the shared socioeconomic pathways: Population scenarios by age, sex and level of education for all countries to 2100, Global Environ. Chang., 42, 181–192, https://doi.org/10.1016/j.gloenvcha.2014.06.004, 2017.
KC., S., Dhakad, M., Potančoková, M., Adhikari, S., Yildiz, D., Mamolo, M., Sobotka, T., Zeman, K., Abel, G., Lutz, W., and Goujon, A.: Updating the Shared Socioeconomic Pathways (SSPs) Global Population and Human Capital Projections, IIASA Working Paper WP-24-003, Laxenburg, Austria, https://pure.iiasa.ac.at/id/eprint/19487/ (last access: 14 July 2026), 2024.
KC, S. (2026a). SSP Population and Human-Capital Projections, 2025-Rebased, 2025-2100 (zen2025V01) [Data set]. Zenodo. https://doi.org/10.5281/zenodo.21738149
KC, S. (2026b). Long-Run SSP Population and Human-Capital Projections, 2025-Rebased, 2100-2300 (zen2300y2025V01) [Data set]. Zenodo. https://doi.org/10.5281/zenodo.21738637
Klein Goldewijk, K., Beusen, A., Doelman, J., and Stehfest, E.: Anthropogenic land use estimates for the Holocene – HYDE 3.2, Earth Syst. Sci. Data, 9, 927–953, https://doi.org/10.5194/essd-9-927-2017, 2017.
Lange, S., Volkholz, J., Geiger, T., Zhao, F., Vega, I., Veldkamp, T., Reyer, C., Warszawski, L., Huber, V., Jägermeyr, J., Schewe, J., Bresch, D., Büchner, M., Chang, J., Ciais, P., Dury, M., Emanuel, K., Folberth, C., Gerten, D., and Frieler, K.: Projecting Exposure to Extreme Climate Impact Events Across Six Event Categories and Three Spatial Scales, Earth's Future, 11, e2020EF001616, https://doi.org/10.1029/2020EF001616, 2020.
Li, F., Lawrence, D. M., Rogers, B. M., Burton, C., Huang, H., Jiang, Y., Kaiser, J. W., Kasoar, M., Lee, H., Leung, R., Nieradzik, L., Wang, A., Ward, D. S., Ce, L., Li, Y., Lin, Z., Voulgarakis, A., and Xue, Y.: The Fire Modeling Intercomparison Project (FireMIP) for CMIP7, Geosci. Model Dev., 19, 3989–4007, https://doi.org/10.5194/gmd-19-3989-2026, 2026.
Luderer G., Weigmann P., Roelfsema M., Creutzig F., Hsu A., Kikstra J. S., Köhler-Schindler L., Lecuyer F., Manya-Gutierrez D., Zhang Z., Reis L. A., Angelkorte G., Baptista L. B., Bondarenko M., Daioglou V., de Boer H.-S., Drouet L., Dürrwächter J., Fricko O., Fu X., Fujimori S., George M., Hagen A. K., Hasegawa T., Joshi S., Mastrucci A., Nishiura O., O'Neill B., Paprotny D., Rosemann R., Schaeffer R., Tavoni M., van Vuuren D., and Riahi K.: Sector-detailed urban Greenhouse Gas Emission Futures derived from the ScenarioMIP-CMIP7 ensemble, Environ. Res. Lett., accepted in print, 2026. [preprint available at https://doi.org/10.5281/zenodo.19348485]
Murakami, D., Yamagata, Y.: Estimation of Gridded Population and GDP Scenarios with Spatially Explicit Statistical Downscaling. Sustain., 11, 2106. https://doi.org/10.3390/su11072106, 2019.

https://doi.org/10.5194/egusphere-2026-5045
Preprint. Discussion started: 15 September 2026

Naik, V., Durack, P. J., Nicholls, Z., Buontempo, C., Dunne, J. P., Hewitt, H. T., Macintosh, C., O'Rourke, E.: Climate models need more frequent releases of input data — here's how to do it. Nature, 644, 874–875, https://doi.org/10.1038/d41586-025-02642-3, 2025.

Nieves, J. J., Sorichetta, A., Linard, C., Bondarenko, M., Steele, J.E., Stevens, F. R., Gaughan, A. E., Carioli, A., Clarke, D. J., Esch, T., Tatem, A. J.: Annually modelling built-settlements between remotely-sensed observations using relative changes in subnational populations and lights at night, Comput. Environ. Urban Syst., 80, 101444, https://doi.org/10.1016/j.compenvurbsys.2019.101444, 2020.

O'Neill, B. C., Kriegler, E., Ebi, K. L., Kemp-Benedict, E., Riahi, K., Rothman, D. S., van Ruijven, B. J., van Vuuren, D. P., Birkmann, J., Kok, K., Levy, M., and Solecki, W.: The roads ahead: Narratives for shared socioeconomic pathways describing world futures in the 21st century, Global Environ. Chang., 42, 169–180, https://doi.org/10.1016/j.gloenvcha.2015.01.004, 2017.

OECD: OECD Geographical Definitions, https://www.oecd.org/en/data/datasets/oecd-geographical-definitions.html, (last access: 25 May 2026), 2026.

Office for National Statistics: Trends in the UK labour share: 1997 to 2023, https://www.ons.gov.uk/economy/economicoutputandproductivity/output/articles/trendsintheuklabourshare1997to2023/2024-11-25, (last access: 26 May 2026), 2024.

OpenStreetMap: https://openstreetmap.org/, (last access: 25 May 2026), 2026.

Paprotny, D. Historical and future population density data for CMIP7 and ScenarioMIP [dataset], https://doi.org/10.5281/zenodo.19353707, 2026.

Paprotny, D., Mengel, M.: Population, land use and economic exposure estimates for Europe at 100 m resolution from 1870 to 2020, Sci. Data, 10, 372, https://doi.org/10.1038/s41597-023-02282-0, 2023.

Paprotny, D.: Exposure datasets at multiple scales, Version v1 [dataset], https://doi.org/10.5281/zenodo.14892500, 2025a.

Paprotny, D.: Exposure datasets at multiple scales, Version v2 [dataset], https://doi.org/10.5281/zenodo.17572467, 2025b.

Paprotny, D.: Historical and future population density data for CMIP7 and ScenarioMIP [dataset], https://doi.org/10.5281/zenodo.19353707, 2026.

Paprotny, D., Hawker, L.: Population density, https://input4mips-cvs.readthedocs.io/en/latest/dataset-overviews/population/, (last access: 15 July 2026), 2026.

Paprotny, D., Tilloy, A., Treu, S., Buch, A., Vousdoukas, M. I., Feyen, L., Kreibich, H., Merz, B., Frieler, K., Mengel, M.: Attribution of flood impacts shows strong benefits of adaptation in Europe since 1950, Sci. Adv., 11, eadt7068, https://doi.org/10.1126/sciadv.adt7068, 2025.

Pesaresi, M., and Politis, P.: GHS-BUILT-S R2023A - GHS built-up surface grid, derived from Sentinel2 composite and Landsat, multitemporal (1975-2030) [dataset], https://doi.org/10.2905/9F06F36F-4B11-47EC-ABB0-4F8B7B1D72EA, 2023.

https://doi.org/10.5194/egusphere-2026-5045
Preprint. Discussion started: 15 September 2026

Pesaresi, M., and Politis, P.: GHS-LAND R2022A - Land fraction as derived from Sentinel2 image composite (2018) and OSM data [dataset], https://doi.org/10.2905/AB7AD451-5ED5-44A6-A4D0-9F7A4E848CEE, 2022.

Pesaresi, M., Schiavina, M., Politis, P., Freire, S., Krasnodębska, K., Uhl, J. H., Carioli, A., Corbane, C., Dijkstra, L., Florio, P., Friedrich, H. K., Gao, J., Leyk, S., Lu, L., Maffenini, L., Mari-Rivero, I., Melchiorri, M., Syrris, V., Van Den Hoek, J., and Kemper, T.: Advances on the Global Human Settlement Layer by joint assessment of Earth Observation and population survey data. International Journal of Digital Earth, 17(1), https://doi.org/10.1080/17538947.2024.2390454, 2024.

Pietroiusti, R., Turco, M., Hetzer, J., Montano, S. P., Laridon, A., Lejeune, Q., Paprotny, D., and Thiery, W.: Increasing lifetime exposure to extreme fire weather under climate change in Europe. Environ. Res. Lett., accepted in print, 2026. [preprint available at https://doi.org/10.31223/X5ZZ0R]

Sauer, I. J., Reese, R., Otto, C., Geiger, T., Willner, S. N., Guillod, B. P., Bresch, D. N., and Frieler, K.: Climate signals in river flood damages emerge under sound regional disaggregation, Nat. Commun., 12, 2128, https://doi.org/10.1038/s41467-021-22153-9, 2021.

Schewe, J., Zantout, K., Gosling, S. N., Hantson, S., Jägermeyr, J., Li, F., Pokhrel, Y., Rabin, S., Reyer, C. P. O., Burek, P., Chang, J., Emanuel, K., Folberth, C., Grillakis, E., Guillaumot, L., Hanasaki, N., Iizumi, T., Ito, A., Kou-Giesbrecht, S., Koutroulis, A., Lampe, S., Li, M., Lin, T.-S., Liu, W., Nyenah, E., Okada, M., Ostberg, S., Park, C. Y., Qi, W., Satoh, Y., Umer, M., Volkholz, J., Zabel, F., Zhu, Q., Büchner, M., Hassel, J., Klar, J., Quesada-Chacón, D., Otto, C., Sauer, I., Frieler, K.: Updated global projections of exposure to six types of climate-related extreme events. Zenodo [preprint], https://doi.org/10.5281/zenodo.21358737, 2026.

Schiavina M., Freire S., Carioli A., MacManus K.: GHS-POP R2023A - GHS population grid multitemporal (1975-2030) [dataset], https://doi.org/10.2905/2FF68A52-5B5B-4A22-8F40-C41DA8332CFE, 2023.

Schoppa, L., Barendrecht, M., Paprotny, D., Sairam, N., Sieg, T., and Kreibich, H.: Projecting flood risk dynamics for effective long-term adaptation, Earth's Future, 12, e2022EF003258, https://doi.org/10.1029/2022EF003258, 2024.

Serres, K., Gámbaro, F., Pietroiusti, R., Da Re, D., Vincenti-Gonzalez, M., da Silva Candido, D., Arsevska, E., De Dixmude, A. J., Quesada, D., Mengel, M., Paprotny, D., Klitting, R., Marsboom, C., Thiery, W., Ghisbain, G., Erazo, D., and Dellicour, S.: Escalating human exposure to tropical mosquito-borne viruses in Europe, bioRxiv [preprint], https://doi.org/10.64898/2025.12.02.691392, 2025.

Statistik Austria: STATcube - Statistische Datenbank, https://www.statistik.at/datenbanken/statcube-statistische-datenbank, (last access: 26 May 2026), 2026.

Stalhandske, Z., Steinmann, C. B., Meiler, S., Sauer, I. J., Vogt, T., Bresch, D. N., and Kropf, C. M.: Global multi-hazard risk assessment in a changing climate, Sci. Rep., 14, 5875, https://doi.org/10.1038/s41598-024-55775-2, 2024.

Steinhausen, M., Paprotny, D., Dottori, F., Sairam, N., Mentaschi, L., Alfieri, L., Lüdtke, S., Kreibich, H., Schröter, K.: Drivers of future fluvial flood risk change for residential buildings in Europe, Glob. Environ. Chang., 76, 102559, https://doi.org/10.1016/j.gloenvcha.2022.102559, 2022.

Thiery, W., Lange, S., Rogelj, J., Schleussner, C.-F., Gudmundsson, L., Seneviratne, S. I., Andrijevic, M., Frieler, K., Emanuel, K., Geiger, T., Bresch, D. N., Zhao, F., Willner, S. N., Büchner, M., Volkholz, J., Bauer, N., Chang, J., Ciais, P., Dury, M., François, L., Grillakis, M., Gosling, S. N., Hanasaki, N., Hickler, T., Huber, V., Ito, A., Jägermeyr, J., Khabarov, N., Koutroulis, A., Liu, W., Lutz, W., Mengel, M., Müller, C., Ostberg, S., Reyer, C. P. O., Stacke, T., and Wada, Y.: Intergenerational inequities in exposure to climate extremes, Science, 374, 158–160, https://doi.org/10.1126/science.abi7339, 2021.

United Nations: National Accounts - Analysis of Main Aggregates (AMA), https://unstats.un.org/unsd/snaama/, (last access: 26 May 2026), 2025.

United Nations: World Population Prospects, https://population.un.org/wpp/, (last access: 26 May 2026), 2024.

Van Vuuren, D. P., O'Neill, B. C., Tebaldi, C., Sanderson, B. M., Chini, L. P., Friedlingstein, P., Hasegawa, T., Riahi, K., Govindasamy, B., Bauer, N., Eyring, V., Fall, C. M. N., Frieler, K., Gidden, M. J., Gohar, L. K., Högner, A., Jones, A. D., Kikstra, J., King, A., Knutti, R., Kriegler, E., Lawrence, P., Lennard, C., Lowe, J., Mathison, C., Mehmood, S., Nicholls, Z., Prado, L. F., Zhang, Q., Rose, S. K., Ruane, A. C., Sandstad, M., Schleussner, C.-F., Seferian, R., Sillmann, J., Smith, C., Sörensson, A. A., Panickal, S., Tachiiri, K., Vaughan, N., Vishwanathan, S. S., Yokohata, T., Zecchetto, M., and Ziehn, T.: The Scenario Model Intercomparison Project for CMIP7 (ScenarioMIP-CMIP7), Geosci. Model Dev., 19, 2627–2656, https://doi.org/10.5194/gmd-19-2627-2026, 2026.

Vertegaal, D. M., van den Hurk, B. J. J. M., Couasnon, A., Aleksandrova, N., Bovenschen, T., Gradiyanto, F., Leijnse, T. W. B., Goulart, H. M. D., and Muis, S.: Climate and impact attribution of compound flooding induced by tropical cyclone Idai in Mozambique, Nat. Hazards Earth Syst. Sci., 26, 1417–1433, https://doi.org/10.5194/nhess-26-1417-2026, 2026.

Winkler, K., Witting, M., Gulde, F., Garschagen, M., Pongratz, J., and Rounsevell, M.: Spatiotemporal scenarios of socioeconomic futures in Germany, Front. Clim., 7, 1715424, https://doi.org/10.3389/fclim.2025.1715424, 2026.

World Bank: DataBank ICP 2021, https://databank.worldbank.org/source/icp-2021, (last access: 26 May 2026), 2026.

World Climate Research Programme: Model Intercomparison Projects (MIPs), https://wcrp-cmip.org/mips/, (last access: 15 July 2026), 2026.